\$5000 ELSEVIER

Contents lists available at ScienceDirect

### Geochimica et Cosmochimica Acta

journal homepage: www.elsevier.com/locate/gca





### Dissolved rare earth elements in the North Pacific Subtropical Gyre: Lithogenic sources and water mass mixing control

Axiang Cao <sup>a,b,1</sup>, Qian Liu <sup>a,1</sup>, Jing Zhang <sup>a,c,\*</sup>, Alan M. Shiller <sup>d</sup>, Yihua Cai <sup>e</sup>, Ruifeng Zhang <sup>f</sup>, Melissa Gilbert <sup>d</sup>, Xianghui Guo <sup>e</sup>, Zhiyu Liu <sup>e</sup>

- <sup>a</sup> Frontiers Science Center for Deep Ocean Multispheres and Earth System, and Key Laboratory of Marine Chemistry Theory and Technology, Ministry of Education, Ocean University of China, Qingdao 266100, China
- <sup>b</sup> College of Chemistry and Chemical Engineering, Ocean University of China, Qingdao 266100, China
- <sup>c</sup> Faculty of Science, Academic Assembly, University of Toyama, Toyama 9308555, Japan
- d School of Ocean Science and Engineering, University of Southern Mississippi, 1020 Balch Blvd., Stennis Space Center, MS 39529, USA
- e State Key Laboratory of Marine Environmental Science and College of Ocean and Earth Sciences, Xiamen University, Xiamen 361000, China
- <sup>f</sup> School of Oceanography, Shanghai Jiao Tong University, Shanghai 200030, China

### ARTICLE INFO

Associate editor: Tim Conway

Keywords: GEOTRACES Rare earth elements North Pacific Subtropical Gyre Lithogenic source Water mass

### ABSTRACT

In the North Pacific Subtropical Gyre, which is one of the largest oligotrophic regions, there is a lack of information regarding the sources and transport of trace metals through water mass mixing. Rare earth elements (REEs) are essential for tracing lithogenic sources and water mass transport. In this study, we present dissolved REE concentrations and the factors controlling their distributions in the northwest Pacific during a GEOTRACES cruise (GP09). In the surface water along 11°N, we observed input signals from the Philippine and the Hawaiian Islands, characterized by positive Eu anomalies and slightly elevated REE concentrations. By incorporating our data and published REE data from the northwest Pacific to the southeast Pacific (40°N-40°S), we demonstrated that the REE concentrations and Yb/Nd ratios can distinguish North Pacific Intermediate Water (NPIW), Antarctic Intermediate Water (AAIW), and modified AAIW. By estimating the ratio of water mass mixing, we suggest that heavy REEs are predominantly contributed by water mass mixing (e.g., 93 %  $\pm$  4% for Yb) and can be used as semi-conservative tracers to quantify the mixing of NPIW and modified AAIW at the potential density of 27.2 kg/m $^3$ . At ~800 m depth at stations K12, K13, and K14, weak negative Ce anomalies (>0.1) were observed, indicating the lateral transport of water masses imprinted with sediment signals from the Philippine Islands. In the deep waters (>1500 m) at the Luzon Strait (station K1), we propose that the weak Ce negative anomalies (>0.08) and low Yb/Nd ratios (<5), combined with the low beam transmission, are the result of particle resuspension and release. In deep water (>2000 m), combining high-resolution REE measurements with water mass analysis, our research reveals that dissolved REEs (except Ce) are dominantly controlled by water mass mixing (e.g.,  $80 \% \sim 100 \%$  for Yb and  $70 \% \sim 100 \%$  for Nd). For the non-conservative behavior, which is not explained by water mass mixing, the residual fraction of heavy REEs (<20 % for Yb) originates from release of sinking particles (organic matter and siliceous particles), while the remaining concentrations of light REEs (<30 % for Nd) may be influenced by a combination of particle release and scavenging processes. These findings highlight valuable information about lithogenic sources and the proportions of REE distributions that are controlled by physical and biogeochemical processes. Moreover, it emphasizes the applicability of heavy REEs as effective tracers for understanding basin-scale water mass mixing in the northwest Pacific.

### 1. Introduction

The North Pacific Subtropical Gyre (NPSG) is one of the largest

oligotrophic regions making it essential to understand the sources and transport of trace metals to accurately understand the processes and mechanisms of the biological pump in oligotrophic oceans (Bruland,

<sup>\*</sup> Corresponding author.

E-mail address: jzhang@sci.u-toyama.ac.jp (J. Zhang).

 $<sup>^{\</sup>rm 1}$  Co-first authors. These two authors contributed equally to this work.

1980; Labatut et al., 2014; Nishioka and Obata, 2017; Letelier et al., 2019; Zheng and Sohrin, 2019). Rare earth elements (REEs, or the lanthanide family) are commonly used to trace the sources and transport of trace elements due to their coherent chemical properties and systematic changes (e.g., Lacan and Jeandel, 2001; Zhang et al., 2008; Grenier et al., 2013; Behrens et al., 2018a, b). For instance, Eu anomalies (the anomaly refers to the deviation of the measured value of one element to the value predicted from two adjacent elements after normalization; see section 2.3) can identify lithogenic influences from islands (Zhang et al., 2008; Fröllje et al., 2016; Behrens et al., 2018b), sediment (Grenier et al., 2013), and hydrothermal sources (Jeandel et al., 2013; Stichel et al., 2018; Paffrath et al., 2021). REEs serve as effective proxies for characterizing water masses and have been employed to quantify water mass mixing in combination with hydrographic parameters (Singh et al., 2012; Che and Zhang, 2018; Zhang et al., 2018; Garcia-Solsona et al., 2020; Liu et al., 2022). Notably, light REEs (LREEs) exhibit higher particle reactivity compared to heavy REEs (HREEs), and the fractionation of LREEs from HREEs can serve as an indicator of mediated particle processes. For instance, particles in hydrothermal plumes preferentially scavenge LREEs, resulting in a high (HREEs/LREEs)<sub>N</sub> ratio (the ratio of HREEs to LREEs after normalization) (Zheng et al., 2016; Behrens et al., 2018b).

The sources and transport of trace elements in the NPSG are complex and varied (Bruland, 1980; Labatut et al., 2014; Nishioka and Obata, 2017; Letelier et al., 2019; Zheng and Sohrin, 2019), with many external sources of material at ocean interfaces. These include inputs from the Hawaiian and the Philippine Islands in the surface and subsurface waters (Amakawa et al., 2004; Behrens et al., 2018a, b), as well as hydrothermal plumes from volcanic vents in the Mariana Trough Region (Von Damm, 1990; Klinkhammer et al., 1994; Tagliabue et al., 2010). However, our understanding of these external sources and their contribution to the seawater in the NPSG is incomplete due to limited data availability for the large northwest Pacific basin. Additionally, the intermediate waters in the ocean play important roles in climate change, which store a large amount of carbon, particularly anthropogenic CO2 from the atmosphere (Tsunogai et al., 1993; Sabine et al., 2004). However, our understanding of the extent of intermediate water from South Pacific intrusion into the North Pacific is limited (Lacan and Jeandel, 2001; Qu and Lindstrom, 2004; Zenk et al., 2005; Wang et al., 2015). It is well-recognized that organic matter remineralization influences the distribution of REEs and other trace elements below the depth of chlorophyll maxima (DCM), particularly in the subsurface and intermediate waters (Fitzsimmons et al., 2015; Behrens et al., 2018a). The relative importance of lateral transport and remineralization for the distribution of REEs is required to be assessed. In deep waters of the West Pacific, the distribution of individual REEs is primarily controlled by conservative water-mass mixing. However, a minor fraction of their concentration is also influenced by non-conservative processes (Behrens et al., 2018b), such as scavenging, release from particles, and benthic input (e.g., Zhang et al., 1994; Nozaki et al., 1999; de Baar et al., 2018). The understanding of these non-conservative processes, particularly in the deep waters of the northwest Pacific, remain limited and highlights the need for further research.

Here, we presented high-resolution profiles of REE data collected from 14 stations in the northwest Pacific and identified the potential lithogenic sources, such as Philippine and the Hawaiian Islands, by determining REE anomalies and ratios associated with trace elements. Furthermore, we deduced the advective processes of intermediate water based on our and published REE data and established HREEs' reliability as tracers for quantifying water mass mixing. Finally, we demonstrated that in deep water, the distribution of all REEs (except Ce) was primarily controlled by water mass mixing, while a minor fraction of nonconservative behavior was observed for all HREEs, linked to the release of sinking particles.

### 2. Materials and methods

#### 2.1. Study area

The study area is located in the oligotrophic western NPSG, primarily from  $11^\circ N - 21^\circ N$  west of  $155^\circ E$ , adjacent to the Philippine Islands. The northwest Pacific is connected to the South China Sea through the Luzon Strait, and station K1 is located in the Luzon Strait (Fig. 1). About eight thousand kilometers east of the Philippine Islands are the Hawaiian Islands.

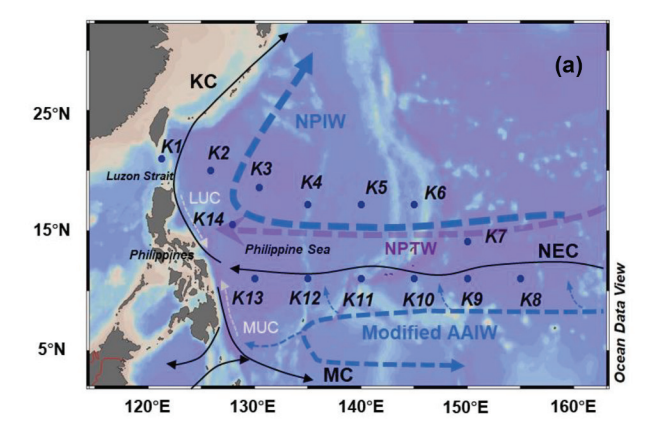
The current field and water mass mixing in the study area are complex. The North Equatorial Current (NEC, Fig. 1a) flowing westward from the East Pacific is the dominant surface current in the study area. Water volume fluxes within the NEC in the western North Pacific are up to 50 Sv ( $10^6 \, \text{m}^3/\text{s}$ ) in the upper 500 m (Toole et al., 1990; Kaneko et al., 1998). The Mindanao Eddy (ME, Supplementary Fig. S1) is a permanent cyclonic mesoscale eddy at the western boundary (Zhang et al., 2012). North Pacific Tropical Water (NPTW) originates from the subtropical Pacific where evaporation dominates over precipitation and is advected westward (Suga et al., 2000; Fig. 1a).

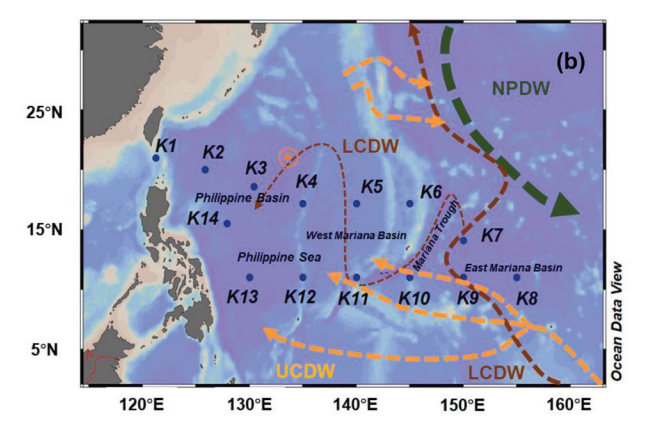
In the study area, the major intermediate water masses are NPIW and the modified AAIW (Fig. 1). NPIW primarily forms in the Sea of Okhotsk and the Gulf of Alaska and is confined to the subtropical gyre of the North Pacific with a neutral density ( $\gamma_n$ ) ranging from 26.5-27.4 kg/m<sup>3</sup> and salinity of 34.0-34.3 (Talley, 1993; Talley et al., 1995; You, 2003). AAIW is formed by the subduction of fresh and cooling Subantarctic Mode Water in the Antarctic convergence region and spreads across the mid-low latitudes of the Pacific Ocean at intermediate depths (McCartney, 1977; Reid, 1997; Bostock et al., 2010; Talley et al., 2011). Around the equator, AAIW undergoes modification due to the upwelled old North Pacific Deep Water, which transforms it into modified AAIW/ EqPIW (Equatorial Pacific Intermediate Water) that have the highest salinities of the intermediate depth waters (Bostock et al., 2010, 2013; Fuhr et al., 2021). A portion of the modified AAIW flows into the North Pacific after crossing the equator (Qu et al., 1998; Qu and Lindstrom, 2004; Zenk et al., 2005), carrying low-salinity, high-oxygen, and REE as identified by Lacan and Jeandel (2001). The convergence of modified AAIW and NPIW takes place near the Philippines Sea and is transported by the intermediate anticyclonic current outside the subtropical gyre (Reid, 1997).

Deep waters of the Pacific Ocean are comprised of North Pacific Deep Water (NPDW), Upper Circumpolar Deep Water (UCDW), and Lower Circumpolar Deep Water (LCDW) (Fig. 1 b). The UCDW reaches the Philippine Sea at 2000–2500 m depth, upwelling at 2000 m (Kawabe et al., 2003, 2009; Kawabe and Fujio, 2010). UCDW is characterized by a neutral density of 27.55 kg/m³  $<\gamma_n<28.0$  kg/m³ (Naveira Garabato et al., 2002), which is similar to the density range of NPDW ( $\gamma_n=27.70–28.01$  kg/m³ (Macdonald et al., 2009; Talley et al., 2011). The western branch of LCDW below 4500 m flows northwestward along the East Mariana Basin, and half of the current enters the West Mariana Basin through the gap around  $11^\circ N$  at  $140^\circ$  E (Kawabe et al., 2003). LCDW has been found at a density between 28.0 kg/m³  $<\gamma_n<28.27$  kg/m³ in the West Pacific (Behrens et al., 2018a).

### 2.2. Sample collection and ancillary data

The seawater samples were collected during the GEOTRACES-CHINA GP09 (KK1903, R/V TAN KAH KEE, April 25 – June 8, 2019) cruise in the northwest Pacific from 14 stations, K1 to K14. Stations K1 and K8 were the key stations, offering a high vertical resolution with  $\sim 48$  layers. The sampling protocol at these stations involved a maximum resolution of 10–20 m above the water depth of 300 m and 100 m below the water depth of 300 m. The remaining stations (K2  $\sim$  K7, K9  $\sim$  K14) were classified as general stations and had a vertical resolution of  $\sim$ 24 layers, covering the full water column. However, these general stations maintained a higher resolution above 300 m, with approximately 9–14





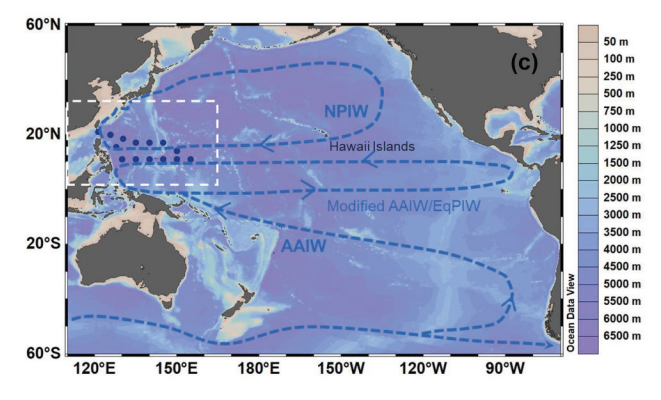


Fig. 1. Map of stations sampled during the GP09 cruise (blue dots) and generalized circulation patterns in this region. (a) Schematic flow patterns of major surface currents (black solid arrows, NEC (North Equatorial Current), MC (Mindanao current), KC (Kuroshio Current)), subsurface currents or water mass (Gray dashed arrows represent the LUC (Luzon Undercurrent), and MUC (Mindanao Undercurrent). Purple dashed arrows represent the NPTW (North Pacific Tropical Water)) and intermediate water masses (blue dashed arrows, modified AAIW (Antarctic Intermediate Water)/ EqPIW (Equatorial Pacific Intermediate Water), NPIW (North Pacific Intermediate Water)). (b) Major deep water masses flow pathways. Green dashed arrows represent the spreading of NPDW (North Pacific Deep Water). Yellow and brown dashed arrows represent the northward flow of UCDW (Upper Circumpolar Deep Water) and LCDW (Lower Circumpolar Deep Water), respectively. The circle with a center point shows upwelling from the UCDW layer to the upper layer (after Kawabe and Fujio, 2010; Jia et al., 2020; Zhai and Gu, 2020; Tian et al., 2021). (c) Location of the study area (dashed boxes) in the Pacific with intermediate current patterns. The blue dots represent stations in this study. Maps were created using Ocean Data View (ODV) software (Schlitzer, 2016).

vertical layers. The seawater was sampled from 12 L Niskin-X bottles with Teflon-liners, which were deployed on an epoxy coated frame equipped with conductivity-temperature-depth sensors (CTD, Sea-Bird 911 plus). Surface water was collected every 6 h using a homemade underway fish-towing system (Zhang et al., 2019) and the stations are marked with TF6 to TF143. Immediately after collection, sample bottles were transferred to a  $\sim$  6 m-long, class-1000, clean container laboratory onboard. Seawater was filtered directly from Niskin-X bottles into Low-Density Polyethylene (LDPE) bottles (500 mL) through Pall AcroPak 1000 cartridge filters. The 0.45  $\mu m$  membrane filters and 0.2  $\mu m$  membrane filters were used for the full water depth samples and the surface samples, respectively. The filtrate was acidified to pH  $\leq$  2 using 6 M ultra-pure hydrochloric acid (Optima grade, Fisher Chemical), and resealed in double bags. The Niskin-X bottles, LDPE sampling bottles, filters, and tubes were all acid-cleaned before use.

Salinity, temperature, and dissolved oxygen (DO) data were obtained by SBE 911plus CTD and DO sensors, respectively. The DO values measured by Winkler spectrophotometry (Labasque et al., 2004) at specific depths agreed with the CTD sensor data. Chlorophyll was measured on a Turner Designs fluorometer following Welschmeyer (1994) after filtering onto Machery Nagel GF/F filter papers.

### 2.3. Rare earth elements analysis

For REE analyses at the Ocean University of China (OUC), 150–180 mL seawater was concentrated using NOBIAS PA1 (Takata et al., 2009; Hatje et al., 2014; Liu et al., 2022) in a class 1000 clean room. To correct for the pre-concentration efficiency of REEs, a known amount of Lu was added into each sample before the pre-concentration procedure. The eluent (2 mL of 1 M nitric acid (HNO $_3$ )) was determined by an inductively coupled plasma-mass spectrometer (ICP-MS, Thermo iCAP Q). Instrumental blanks of 2 % HNO $_3$  were measured and deducted from each sample. The stability of ICP-MS measurements was checked by the analysis of 0.1 ng/mL REE standards every ten samples. Rhodium, indium, and rhenium in a 2 % nitric acid solution (10 ng/mL) were added to each sample as an internal standard for correcting matrix effects and any instrumental sensitivity drift.

Average procedural blank values (n = 20) represented less than 3 % of the concentration in surface water (n = 4), which is usually the lowest concentration in the ocean (except for La = 4.1 %). The concentration of Ce is typically low in deep water, with blank values accounting for less than 3 % of the measured Ce concentration in seawater at a depth of 4000 m (n = 11). Recoveries of Lu in all samples were greater than 90 %. The relative standard deviations (1 $\sigma$  RSD) of mean REE concentrations determined by replicate analysis of Pacific surface water (n = 4) and deep water (4000 m, n = 11) were both less than 5 %. The measurement error of each sample is reported in Supplementary Tables S1 and S2.

The Eu anomaly (Eu/Eu\*) was calculated as Eu/Eu\* =  $3(Eu)_N/(2 \times (Sm)_N + (Tb)_N)$  (Zhang et al., 2008), where (REE)\_N refers to the Post Archean Australian Shale (PAAS) (Taylor and McLennan, 1985) normalized REE. Eu\* refers to the value predicted from Sm and Tb after normalization. The Ce anomaly (Ce/Ce\*) was calculated as Ce/Ce\* =  $(Ce)_N/(2 \times (Pr)_N - (Nd)_N)$  (Garcia-Solsona et al., 2014). Ce\* represents the expected or normalized value of Ce based on the pattern of Pr and Nd. The relative standard deviations of Pacific deep water (4000 m, n = 11) for Eu/Eu\* and Ce/Ce\* are 3.3 % and 5.0 %, respectively. By convention, an anomaly value > 1 (or < 1) is referred to as a positive (or negative) anomaly. Yb/Nd ratio was calculated as  $(Yb)_N/(Nd)_N$  with a standard deviation of Pacific deep water (4000 m, n = 11) of 3.7 %.

To demonstrate the reliability of the data, seawater samples collected during this cruise were also measured at the University of Southern Mississippi (USM). The seawater samples were pre-concentrated using a SeaFAST system (offline mode, Elemental Scientific, Inc) and spiked with Nd-145, Sm-149, Eu-153, Gd-155, Dy-161, Er-167, and Yb-171. Detailed methods are available on www.bco-dmo.org/dataset/651138. The correlation coefficients ( $\mathbb{R}^2$ ) of the data sets between the two

laboratories are  $\geq$ 0.99 for all elements except La and Ce (Supplementary Table S3). Considering that La and Ce are susceptible to contamination, the R² of 0.96 for La and 0.86 for Ce are acceptable. In addition, the multiple isotopic elements were used as internal standards for REEs analysis at the USM. The agreement between the two data sets demonstrates the reliability of using single HREE (Lu) as an internal standard for the calibration of LREEs. For internal consistency, the figures and calculations below rely only on the OUC data.

### 2.4. Water mass analysis

To facilitate comparisons with previous studies and to achieve a comprehensive analysis, we selected the identical water layer density (a potential density  $(\sigma_\theta)$  of 27.2 kg/m³) as employed by Qu and Lindstrom (2004) and Wang et al. (2015) to investigate the northward intrusion of AAIW. The mixing ratios of three water masses (NPDW, UCDW, and LCDW) below 2000 m were determined using potential temperature and salinity. The equations are as follows (Li et al., 2021a, 2021b; Li et al., 2022; Cao et al., 2023), which are developed from the optimum multiparameter method (Tomczak and Large, 1989; Karstensen and Tomczak, 1998);

$$\sum_{i=1}^{n} f_i = 1 + R_M \tag{1}$$

$$\sum_{i=1}^{n} f_i \theta_i = \theta_{obs} + R_{\theta} \tag{2}$$

$$\sum_{i=1}^{n} f_i S_i = S_{obs} + R_S \tag{3}$$

$$\Delta Nd = Nd_{obs} - \sum_{i=1}^{n} f_i Nd_i$$
 (4)

$$\Delta Yb = Yb_{obs} - \sum_{i=1}^{n} f_i Yb_i \tag{5}$$

where,  $f_i$  represents the fraction of the water mass. For the intermediate water, to estimate AAIW intrusion ratio along a certain potential density (27.2 kg/m<sup>3</sup>), we assumed a two end-members mixing model (modified AAIW and NPIW), i.e. the subscripts i = 2. For the deep water, we applied a three end-members mixing model (NPDW, UCDW, and LCDW), subscripts i = 3. The first equation is mass conservation. The  $\theta_i$ S<sub>i</sub>, Nd<sub>i</sub>, and Yb<sub>i</sub> are the potential temperatures, salinities, dissolved Nd, and dissolved Yb concentrations of the end member water samples. The subscript "obs" represents the observed values. The R is residual. The calculated results were derived using the non-negative least-squares regression method to minimize the residuals (Tomczak and Large, 1989; Karstensen and Tomczak, 1998). For each data point in water mass analysis, the residuals of the mass equation  $(R_M)$  were less than 1 %.  $\Delta Nd$ and  $\Delta Yb$  are defined as the differences between the observed concentrations and the concentrations calculated from physical mixing of the end-members. A positive value of  $\Delta Nd$  (or  $\Delta Yb$ ) indicates an increase in the concentration of Nd (or Yb) beyond what can be accounted by water mass mixing alone. This implies the presence of additional sources or release processes. Conversely, a negative value suggests a decrease in the Nd (or Yb) concentration beyond that expected from water mass mixing, signifying the influence of sinks or scavenging processes.

For the intermediate water, the modified AAIW end-member was represented by stations GeoB17015  $\sim$  GeoB17018 at a potential density of 27.2 kg/m $^3$  (Behrens et al., 2018b). The NPIW end-member was defined by stations P1-1  $\sim$  P1-4 in the region between 37 and 40°N in the North Pacific (Cao et al., 2023). The end member values for both modified AAIW and NPIW are listed in Table 1. Station K1 was excluded from the two end-members mixing model due to a mixing from the South China Sea intermediate water.

For the deep water, end-members were selected from stations located

**Table 1**Hydrographic characteristics and concentrations of REEs in modified AAIW and NPIW.

water mass	Modified AAIW	NPIW
Potential temperature (°C)	$5.70 \pm 0.2 \ (n=4)$	$3.85 \pm 0.18 \ (n=4)$
Salinity	$34.50 \pm 0.02  (n=4)$	$34.23 \pm 0.02  (n=4)$
Nd (pmol/kg)	$8.3 \pm 0.5 \ (n=4)$	$19.0 \pm 0.9 \ (n=4)$
Yb (pmol/kg)	$4.4 \pm 0.03 \ (n=4)$	$6.8 \pm 0.7 \ (n=4)$
Station	GeoB17015~	P1-1~P1-4
	GeoB17018	(37°N~40°N, 150°E)
	(2°N~8.2°S, 158°E~166°E)	
Reference	Behrens et al., 2018b	Cao et al., 2023

in the region before entering the northwest Pacific Ocean or the Philippine Sea, as water mass properties may undergo changes during transport from the formation region to the study area. For the selection of Nd and Yb, the NPDW end-member consisted of stations north of 25°N, with a neutral density range of 27.70–28.01 kg/m³ (stations P1-1  $\sim$  P1-15; Cao et al., 2023). UCDW and LCDW end-members were chosen from stations south of 11°N, with neutral densities range of 27.55–28.01 kg/m³ and 28.0–28.27 kg/m³, respectively (Behrens et al., 2018b). To obtain hydrographic end-members that closely approximated the mean values of the water masses, we utilized a large amount of potential temperature and salinity data available from WOCE (World Ocean Circulation Experiment, https://www.ewoce.org) stations, located near the REE end-member locations and depths (determined by neutral density). The detailed values and locations of the end-members can be found in Table 2.

### 3. Results

Sampling stations with full water column and hydrographic properties are presented in Figs. 1 and 2, respectively. Detailed data of hydrographic parameters and concentrations of REEs are listed in Supplementary Table S1. Based on the geographical locations, we focus on two transects (Fig. 3), transect "N" (stations K1-K8) and transect "S" (stations K1, K2, K8-K14). Sampling stations for surface water are presented in Fig. 4 and detailed data are listed in Supplementary Table S2. There is a high degree of linear relationship between the Nd concentrations and the sum of LREEs (from La to Sm, except for Ce, which has

**Table 2**Locations of water masses (NPDW, UCDW, and LCDW) and their end-member characteristics including uncertainties.

water mass	NPDW	UCDW	LCDW
Potential temperature (°C)	$1.48 \pm 0.02 \ (n = 21)^a$	$2.22 \pm 0.53 \; (n = 91)^b$	$1.07 \pm 0.078 \; (n = 29)^c$
Salinity	$34.65 \pm 0.003 \text{ (n}$ = $21)^a$	$34.63 \pm 0.03 \text{ (n} = 91)^{b}$	$34.69 \pm 0.005$ (n = 29) <sup>c</sup>
Location	25.17°~34.93°N, 141.2°~149.3°E	-4.7°~3.0°N, 164°~164.99°E	-4.7° ~3.0° N, 164° ~164.99° E
Nd (pmol/kg)	$23.2 \pm 2.4 \ (n=9)^d$	$10.2 \pm 1.1 \; (n = 4)^e$	$28.2 \pm 3.1 \; (n = 14)^f$
Yb (pmol/kg) Location	$9.6 \pm 0.4 \ (n=9)^d$ $25^{\circ} \sim 40^{\circ} N, 150^{\circ} E$	$5.6 \pm 0.4 \text{ (n = 4)}^{\text{e}}$ -15.2° ~6.8° N,	$9.6 \pm 0.5 \text{ (n} = 14)^{\text{f}}$ -8.2°~6.8°N,
		154.2°∼173.5°E	154.2°∼166.1°E

a: Mean values from P10 transect with neutral density of 27.70-28.01 kg/m<sup>3</sup> (WOCE dataset, http://www.ewoce.org).

b: Mean values from P13 transect with neutral density of 27.55-28.01 kg/m<sup>3</sup> (WOCE dataset, http://www.ewoce.org).

c: Mean values from P13 transect with neutral density of 28.0-28.27 kg/m<sup>3</sup> (WOCE dataset, http://www.ewoce.org).

d: Mean values from stations P1-1~P1-15 (2000 m) (Cao et al., 2023).

e: Mean values from station GeoB170014 ( $1002\,m$ ), GeoB170018 ( $1002\,m$ ), and GeoB170019 ( $1002\text{-}1300\,m$ ) (Behrens et al.,  $2018\,b$ ).

f: Mean values from stations GeoB170014 (>3000 m), GeoB170017 (>3000 m), and GeoB170018 (>3400 m) (Behrens et al., 2018b).

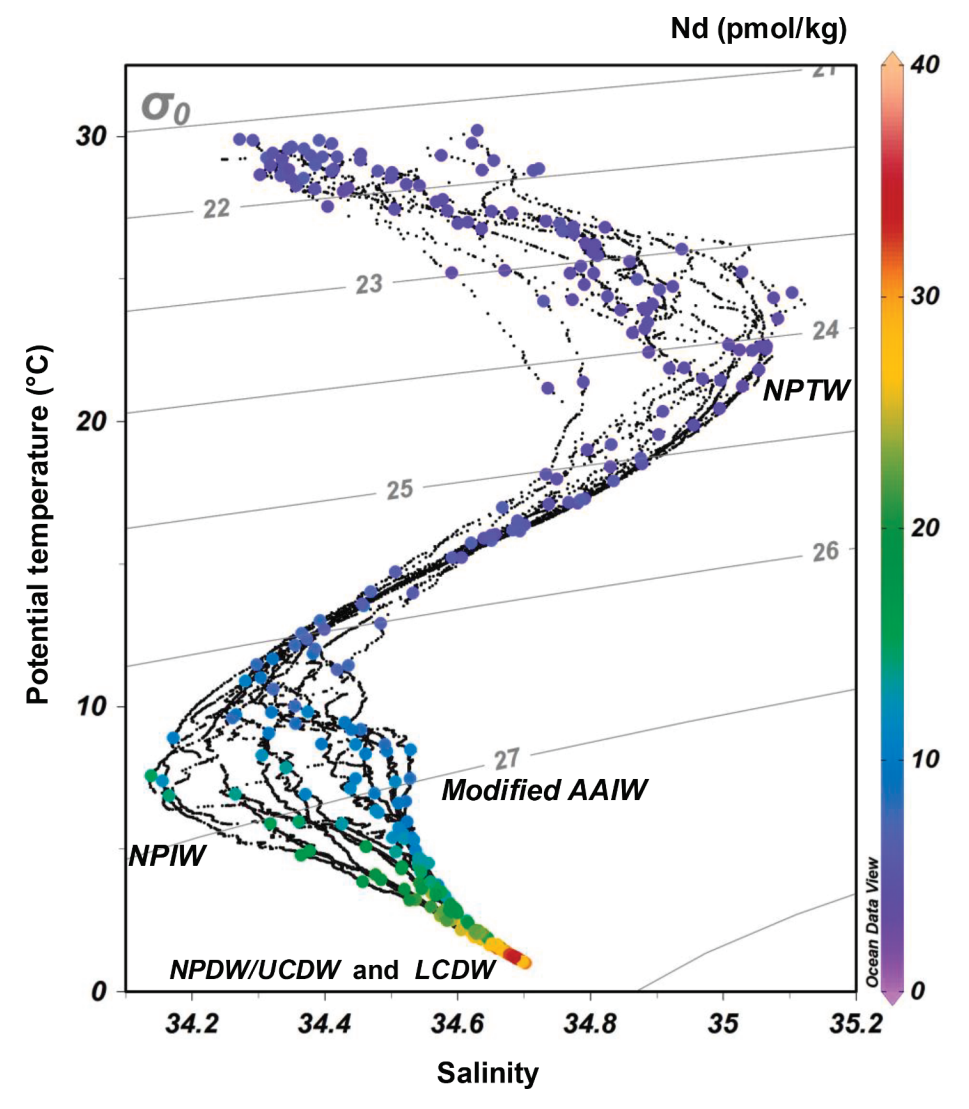


Fig. 2. Potential temperature (°C)-salinity diagram with potential density (kg/m³) contours as solid grey lines. The identified major water masses (NPTW: North Pacific Tropical Water, WPTW: West Pacific Tropical Water, NPIW: North Pacific Intermediate Water, modified AAIW: Antarctic Intermediate Water, NPDW: North Pacific Deep Water, UCDW: Upper Circumpolar Deep Water, and LCDW: Lower Circumpolar Deep Water) are marked at general location based on their hydrographic properties. Colored symbols represent the Nd concentration (pmol/kg) of distinct water samples.

significant redox behavior that the other LREEs do not have) with a correlation coefficient of 0.99. Similarly, the Yb concentrations and the sum of HREEs (from Ho to Lu) exhibit a perfect positive correlation with a coefficient of 1. Moreover, the vertical distributions of a single element and the summed display comparable characteristics (Supplementary Figs. S2 and S3). In the following description of the REE concentrations, we use Nd as a representative for LREEs and Yb for the HREEs.

### 3.1. Hydrographic setting

In the surface layer, potential temperatures ranged from 28.5 °C to 30.2 °C, gradually decreasing through the thermocline at depths exceeding 400 m. Beyond 1000 m, it plummeted to below 5 °C, reaching its lowest point of approximately 1 °C in the bottom water. The salinity increased to a maximum value (>34.79) at 120–180 m and then decreased to a minimum value (<34.25) at 230–640 m. The thermocline in higher latitude waters (stations north of 11°N) was thicker than at lower latitudes (stations at 11°N). The salinity in deep water (>1000 m) increased slowly with depth to about 34.70 and increased to about 34.63 at station K1. For stations north of 11°N (stations K1-K7, K14), the salinity ranged from 34.15 to 35.04, whereas for stations at 11°N

(stations K8-K13), it varied between 34.28 and 35.08.

According to the hydrographic characteristics (salinity and density), we classify six major water masses: NPTW, NPIW, modified AAIW, NPDW, UCDW, and LCDW (Fig. 2). NPTW is identified by a subsurface salinity maximum and is mainly centered at ~180 m to the north of 11°N (S > 34.60, Fig. 3a and e). At intermediate water depths, an NPIW core with a minimum salinity (<34.3, Fig. 3a and e) was observed at  $\sim$ 600 m depth to the north of 11°N. Modified AAIW was defined as a water sample with a potential density between 27.20 and 27.30 kg/m<sup>3</sup> (Zenk et al., 2005,  $\gamma_n = 27.35$  to 27.38 kg/m<sup>3</sup>), and its salinity was almost constant between 34.51 and 34.53 at ~11°N (Fig. 3e). For deep waters (>1000 m), UCDW and NPDW have similar ranges of neutral density. According to previous studies (Naveira Garabato et al., 2002; Macdonald et al., 2009), we regarded seawater with neutral density between 27.55 kg/m  $^3<\gamma_n<28.01~kg/m^3$  as NPDW/UCDW mixed water (Fig. 3a and e). Below 1000 m at station K1, the deep water from the Pacific sinks into the South China Sea through the Luzon Strait. In our study area, LCDW was determined based on high salinities (>34.70; Kawabe et al., 2003; from 4500 m to the seafloor at stations K7, K8, K9; Fig. 3a and e).

Below the intermediate water, as suggested by currents (color and

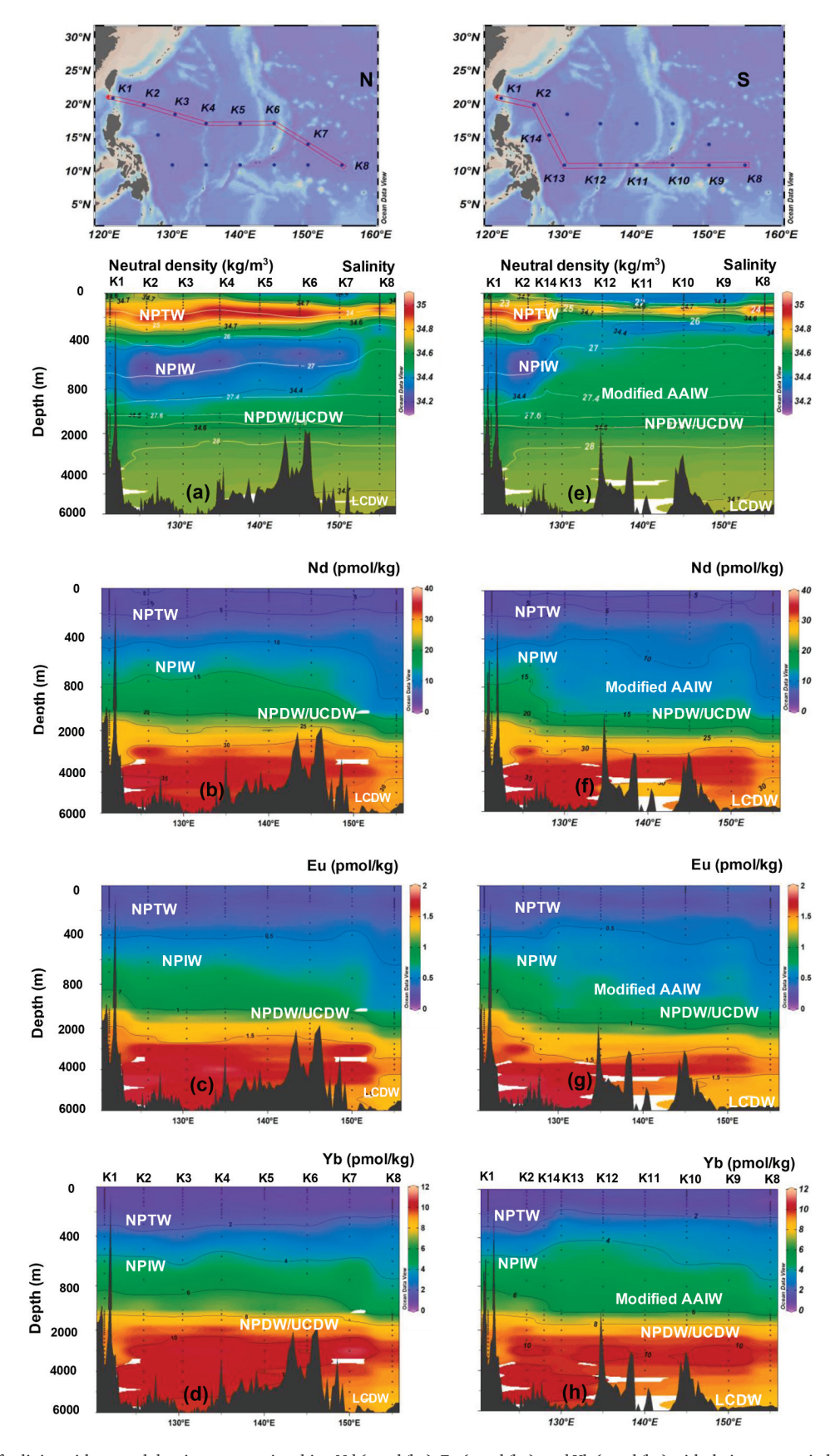


**Fig. 3.** Distribution of salinity with neutral density contours in white, Nd (pmol/kg), Eu (pmol/kg), and Yb (pmol/kg) with their contours in black along the transects N and S. Left panels (a, b, c, and d) display profiles along the transects N, whereas right panels (e, f, g, and h) display profiles along the transects S. (The "N" transect included stations K1-K8 and the "S" transect included stations K1, K2, and K8-K14).

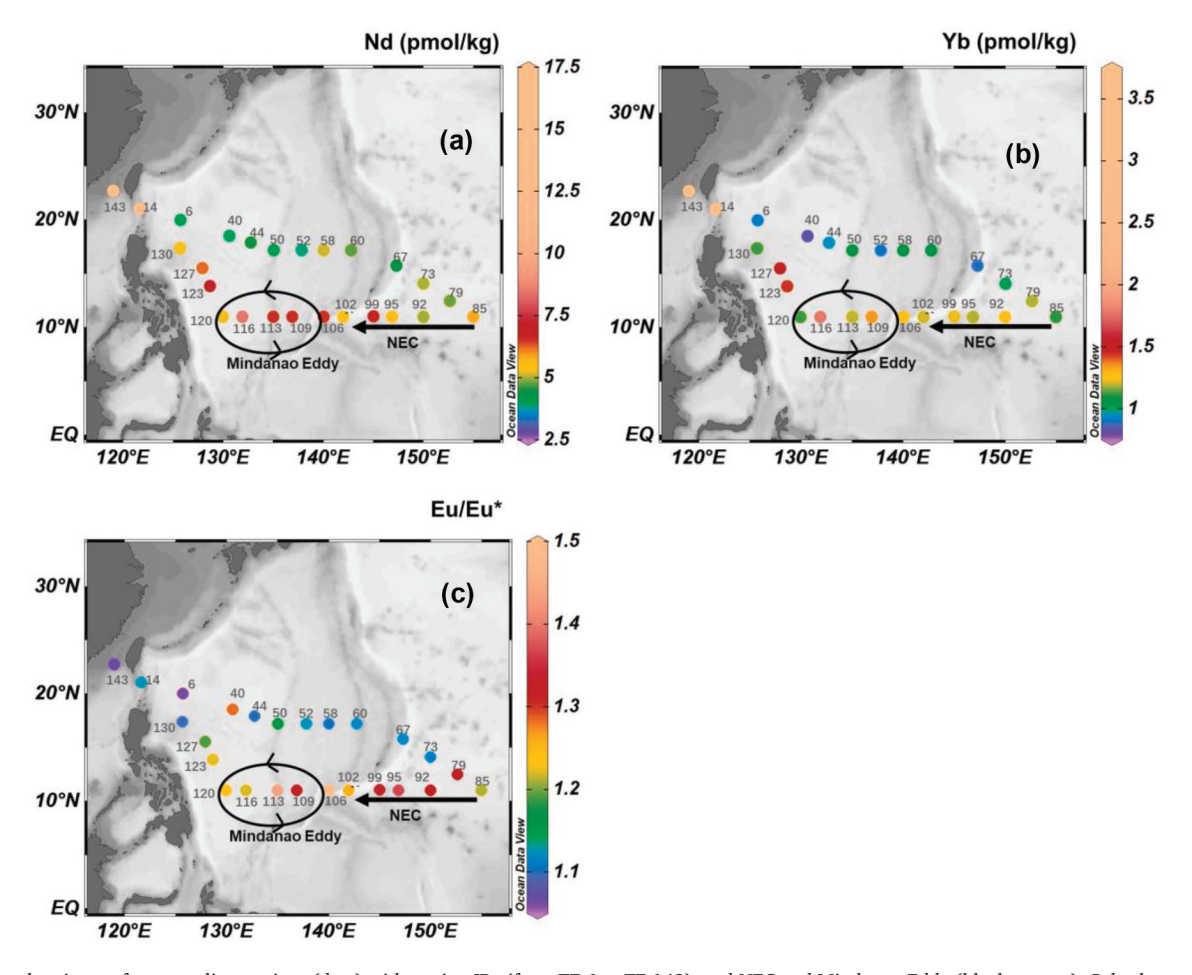


Fig. 4. Maps showing surface sampling stations (dots) with station IDs (from TF-6 to TF-143), and NEC and Mindanao Eddy (black arrows). Color bar represents (a) Nd (pmol/kg), (b) Yb (pmol/kg), and (c) Eu/Eu\* in the surface layer.

arrows) at  $\sim$ 1000 m depth during May (Supplementary Fig. S4), there was an anticyclonic eddy in the sub-thermocline ( $\sim$ 1000 m) between station K13 and the Philippine Islands.

### 3.2. REE concentrations

The concentrations of Nd and Yb in the full water column are shown in Figs. 3 and 5. The REE concentrations at station K8, the farthest site from the coast, were the lowest, ranging from 3.7 to 31.5 pmol/kg for Nd and 0.7-10.0 pmol/kg for Yb. The concentrations of REEs in other stations were relatively high, ranging from 3.6 to 35.3 pmol/kg for Nd and 0.8-10.9 pmol/kg for Yb. REE concentrations were lower in the upper water column (<300 m) (3.6-7.9 pmol/kg for Nd and 0.7-2.6 pmol/kg for Yb) and increased with a depth below 300 m. At stations K7-K14, the concentrations of Nd and Yb increased more slowly than at stations K2-K6. The concentration of Nd reached a maximum at ≥ 4000 m (28.2–35.3 pmol/kg) and Yb at  $\geq$  3000 m (8.3–10.9 pmol/kg). At station K1, compared with other stations at the same water depth, the Nd concentrations were higher at 1300 m  $\sim$  2000 m but lower at 2000 m  $\sim$ 3400 m. Similarly, Yb concentrations were also low below 2000 m at station K1. The distributions of Eu, as shown in Figs. 3 and 5, exhibited similar characteristics to Nd and Yb, i.e., low concentrations in the upper water column (<300 m) and high concentrations in the deep water, and lower concentrations at station K8 than at other stations. The distribution of Eu at station K1 is similar to that of Nd.

The location of station K9 (11°N, 150°E) in our study is in close proximity to station GeoB17011 (10.63°N, 148.90°E) from GEOTRACES Process Study GPpr04 (Behrens et al., 2018b). The two sites exhibited

comparable REE concentrations in layers where hydrographic characteristics (potential temperature, salinity, and dissolved oxygen) closely align, spanning the same or similar sampling depths (from 500 m to 5000 m) (Supplementary Fig. S5). The average differences were 6 % for La, 21 % for Ce, and  $-5\%\pm3\%$  for other REEs (Supplementary Table S4), with negative values indicating lower results compared to Behrens et al., (2018b). Notably, our results for Ce showed good agreement with those of USM (average difference of 8 %), despite some variations in Ce concentrations when compared to station GeoB17011.

Cao et al. (2023) presented data collected at stations P1-26 (150°E, 15°N) and P1-28 (150°E, 13°N), which are in close proximity to station K7 (150°E, 14.1°N). The vertical profiles of Nd and Yb concentrations observed at these three stations exhibited similarity (Supplementary Fig. S6). Depths of 2000 m with close hydrographic properties (potential temperature, salinity and dissolved oxygen) were carefully selected for comparison, and RSDs of 6 % and 1 % were found for Nd and Yb, respectively.

A plume of high Yb/Nd ratios (greater than 6) was distributed from  $\sim\!400\text{--}2000$  m at stations K7-K14 (Fig. 6). A plume of low Dy/Er values (less than 0.6) was distributed from  $\sim\!200$  to 3000 m at stations K8-K14 (Fig. 6). Ce anomalies were all less than 1 (from 0.03 to 0.63) (Fig. 7). At 300–800 m, it rapidly decreases to below 0.08, showing a strong negative anomaly. However, Ce anomalies were more than 0.08 at 1000–2600 m in K1 (0.09  $\sim$  0.11) and 750–1000 m in K12 and K13 (0.11  $\sim$  0.17), which showed a less negative anomaly. At 800–1000 m in station K14, there were also slight increases in Ce anomalies (0.10  $\sim$  0.11).

As shown in Fig. 4, in the surface water, the two stations (TF-0014

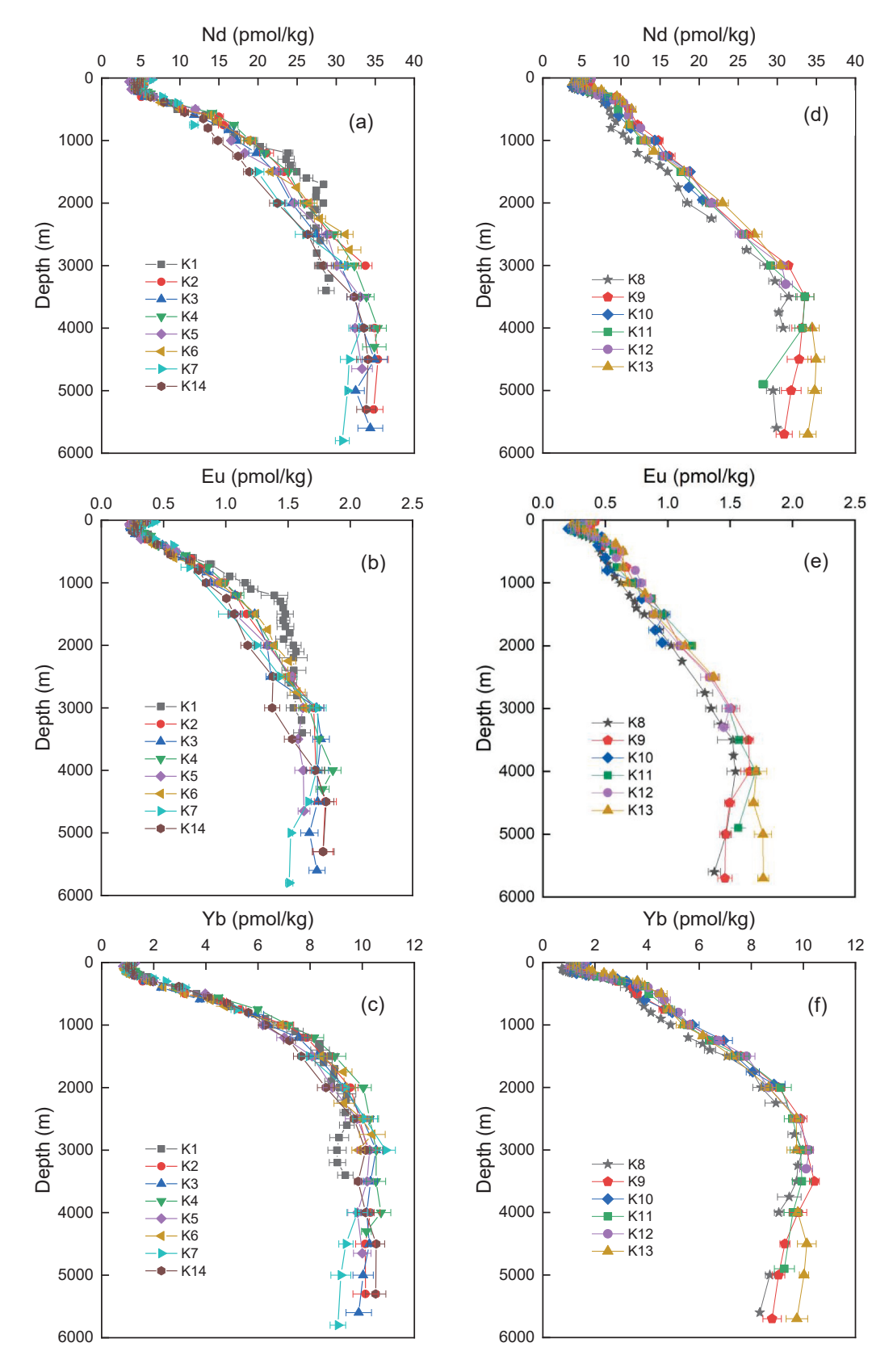


Fig. 5. Vertical profiles of Nd (pmol/kg), Eu (pmol/kg), and Yb (pmol/kg) from all stations. Left panels (a, b, and c) display profiles from the stations north of  $11^{\circ}$ N, whereas right panels (d, e, and f) show stations along  $11^{\circ}$ N.

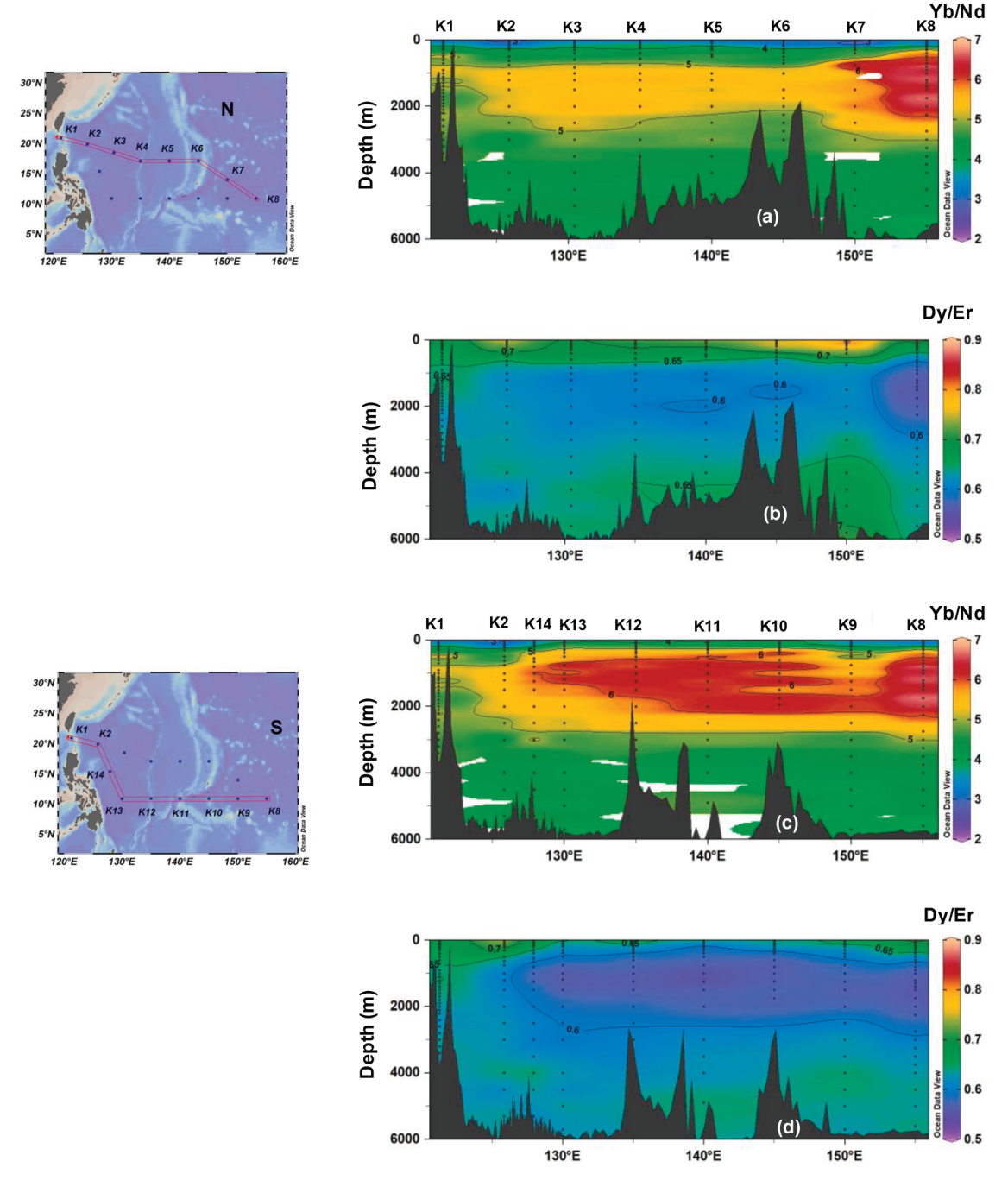


Fig. 6. Distributions of the Yb/Nd and Dy/Er ratios along the transects "N" (a and b) (upper panels) and "S" (c and d) (bottom panels).

and TF-0143) near the South China Sea had the highest REEs (Nd = 15.3  $\pm$  2.3 pmol/kg, Yb = 3.6  $\pm$  0.01 pmol/kg) and the low Eu anomalies (1.1  $\pm$  0.04), which may be influenced by terrestrial source materials. At stations TF-6  $\sim$  TF-73, the REEs and Eu anomalies were depleted (Nd = 4.4  $\pm$  0.5 pmol/kg, Yb = 1.0  $\pm$  0.1 pmol/kg, Eu/Eu\* = 1.1  $\pm$  0.06). Whereas, at stations TF-79  $\sim$  TF-130, the REEs and Eu anomalies were elevated (Nd = 6.1  $\pm$  1.0 pmol/kg, Yb = 1.3  $\pm$  0.2 pmol/kg, Eu/Eu\* = 1.3  $\pm$  0.1).

### 4. Discussion

### 4.1. Modification of Eu anomalies by the islands and lateral transport

At  $\sim 11^{\circ} N$ , we found a stronger positive Eu anomaly (>1.2), and

higher Nd and Yb concentrations at surface water than northern stations (Fig. 4), which is considered to be a tracer for inputs of mantle-derived lithogenic material. We suggest that the Eu anomaly could be the Philippine Islands signal caught up in the Mindanao Eddy since the elevated Eu anomalies ( $1.5 \pm 0.2$ , Supplementary Fig. S7) have been observed in the Philippine Islands (GEOROC database, http://georoc.mpch-mainz.gwdg.de/georoc/). In the equatorial Pacific, surface waters are influenced by riverine inputs from Papua New Guinea (PNG), resulting in slightly elevated REE concentrations and Eu anomalies ( $1.15 \sim 1.20$ , Behrens et al., 2018b). The importance of riverine inputs from Papua New Guinea was also identified through the enrichment of MREEs in surface waters north of PNG (Sholkovitz et al., 1999). In contrast, river input from the east coast of the Philippine Islands was not considered to be a source of REEs in this study due to the lack of large rivers. We

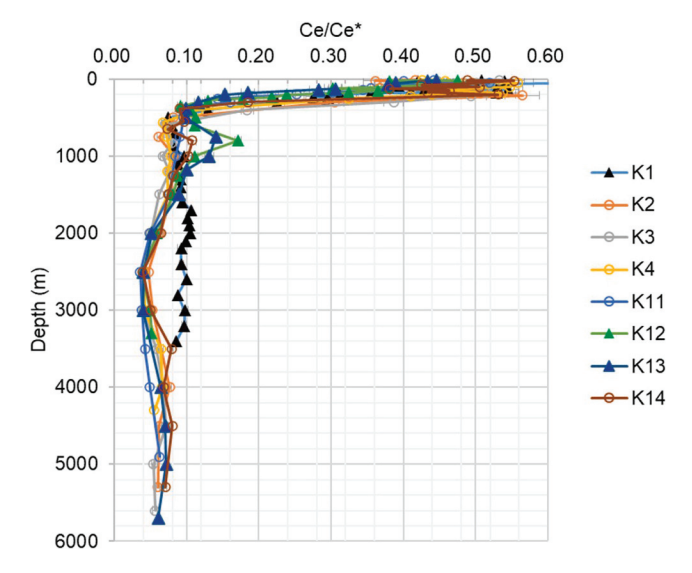


Fig. 7. Vertical profiles of Ce/Ce $^*$  value with error bar. The relative standard deviations for Ce/Ce $^*$  in each sample were less than 7.3 %.

suggest that the surface seawater at  $\sim 11^\circ N$  was affected by the dissolution of solids at the continent/ocean interface.

In addition, this Eu/Eu\* signal might be derived from the Hawaiian Islands where the Eu anomaly of rocks (including pillow lava, picrite, olivine basalt, etc.) is 1.7  $\pm$  0.1 (n = 28) (Zindler et al., 1979; Ren et al., 2009) and lithogenic material is transported by the NEC. Amakawa et al. (2004) also determined that the radiogenic Nd isotope in the surface water of the NEC is supplied by the mantle-derived volcanic rocks of the Hawaiian Islands. Furthermore, the particle trajectory density computed by the particle tracking simulation (Supplementary Fig. S8) also demonstrates that Hawaiian Islands material has a strong influence on waters at 11°N, even though the islands are located further north (18°54′N  $\sim 28^{\circ}15'$  N. The modification of REEs in surface water by the Hawaii Islands is suggested to be the result of weathering of basalt particles (Fröllje et al., 2016). Our study reveals elevated concentrations of REEs in surface water at stations near ~ 11°N compared to the northern stations (Fig. 4a and b). However, previous research on dust fluxes and atmospheric Nd fluxes in the Pacific has shown that these fluxes are higher at high latitudes (13-23°N) compared to low latitudes (5°S-13°N) (Jickells et al., 2005; Hongo et al., 2006). This suggests that atmospheric contributions are not significant in comparison to inputs from the islands, further supporting our findings.

If we assume that the differences in REE concentrations between the surface water at ~11°N and northern stations are solely due to inputs from the Philippine and Hawaii Islands, the Nd and Yb attributed to the islands are 1.7  $\pm$  1.1 pmol/kg and 0.3  $\pm$  0.2 pmol/kg, respectively (the differences in average concentrations of Nd and Yb between stations at  $\sim 11^{\circ} N$  and the northern stations). Studies have shown that PNG is a significant source of REEs in the Tropical Western Pacific (Sholkovitz et al., 1999; Grenier et al., 2013; Behrens et al., 2018b, 2020). Compared to the stations GeoB17014 and GeoB17018, which were unaffected by the PNG input, the addition of Nd and Yb to surface water at stations GeoB17015, GeoB17016, and GeoB17017 by PNG Islands was 1.4  $\pm$  0.4 pmol/kg and  $0.5 \pm 0.2$  pmol/kg, respectively (Behrens et al., 2018b). The REEs values derived from the Philippines and Hawaii Islands to surface waters in the western Pacific account for 20-30 % of the total concentration, which is comparable to the contribution from the PNG Islands. This rough comparison suggests that the Philippine/Hawaii Islands, like the PNG Islands, may be a crucial source of REEs to surface

### 4.2. Controlling factors of REEs in subsurface water to the north of $11^{\circ}N$

NPTW is formed in the oligotrophic area and carries high salinity waters from the subtropical surface to the subsurface (Suga et al., 2000), and is mainly distributed at 300 m and shallower north of 11°N (Fig. 3a and e). The lower interface of the DCM was located at approximately 160 m water depth ( $\sigma_\theta = 24~\text{kg/m}^3$ ) and the factors influencing Nd and Yb at depths above the layer were different than from below.

Above 160 m, as shown in Fig. 8c and f, the absence of a correlation between REEs (Nd and Yb) and salinity implies that REEs are not governed solely by water mass mixing. The minimum concentration of Nd appears at and just below the DCM (~160 m), which has also been observed in the Eastern North Atlantic and the Central Pacific, and is interpreted as scavenging by sinking particles (Stichel et al., 2015; Fröllje et al., 2016). In addition, a few studies have demonstrated the removal of REEs by other processes, such as the uptake of LREEs by methanotrophs (Shiller et al., 2017) and the adsorption of HREEs by Bacillus subtilis and Escherichia coli (Takahashi et al., 2005). Both particle removal and microbial activity may contribute to the general depletion of REEs in the surface water in open oceans. Below 160 m, REEs (Nd and Yb) were negatively correlated with salinity (Fig. 8c and f) and positively correlated with apparent oxygen utilization (AOU) (Fig. 8b and e), which usually represents the oxygen utilized during remineralization processes. This indicates that REEs were controlled by both lateral transport of water masses and organic matter remineralization. Multiple regression analyses for the concentrations of REEs with salinity (for Nd,  $\beta = -0.688$ , p < 0.01; for Yb,  $\beta = -0.675$ , p < 0.01) and AOU (for Nd,  $\beta$ = 0.300, p = 0.021; for Yb,  $\beta = 0.373$ , p < 0.01) showed that water mass mixing was the main factor controlling REEs (the absolute of value  $\beta$  can be used to estimate the relative importance of the parameters to REEs), while remineralization was the secondary factor.

Previous studies have suggested that REEs in NPTW are mainly controlled by water mass mixing (Behrens et al., 2018a, b). However, in this study area, within NPTW, it is proposed that water mass mixing is the main factor controlling REEs below the DCM layer, but not in the upper layers.

## 4.3. Effects of biological processes and water mass transport on the distribution of REEs in the intermediate water

### 4.3.1. Biological processes involved

NPIW was mainly found north of 11°N (stations K1-K7, K14, 300–900 m). Nd vs. AOU and Yb vs. AOU in NPIW are both positively correlated (P < 0.01, Fig. 8a and d), indicating that REEs in NPIW are influenced by the remineralization of organic matter. Remineralization is also an important source of REEs to NPIW north of 20°N (Behrens et al., 2018a, b; Cao et al., 2023). These results demonstrate the critical role of organic matter remineralization on REEs in the NPIW. At  $\sim\!11^\circ\text{N}$ , concentrations of REEs in modified AAIW were relatively constant (Nd  $=11.2\pm1.2$  pmol/kg, Yb  $=4.8\pm0.4$  pmol/kg, 750–800 m), suggesting that REEs in this water mass were conservative. This difference between NPIW and modified AAIW could be due to the different vertical sinking flux of particulate organic matter (POM) since the modified AAIW is largely beneath NPIW, and the sinking flux of POM rapidly decreases with depth (Kishi et al., 2004).

### 4.3.2. Advective processes deduced from REEs

At the intermediate water ( $\sigma_{\theta}=27.2 \text{ kg/m}^3$ ), NPIW was characterized by the minimum salinities in the North Pacific. Similarly, AAIW in the South Pacific was distinguished by low salinity that increases slightly northward towards the equator (Fig. 9a). The distribution characteristics of potential temperature were similar to salinity (Fig. 9b). Based on the location of different hydrographic settings, the Pacific Ocean is divided into four sub-regions (Fig. 9f), namely, the NPIW formation region(S < 34.3), AAIW formation region (S = 34.2  $\sim$  34.35, Bostock

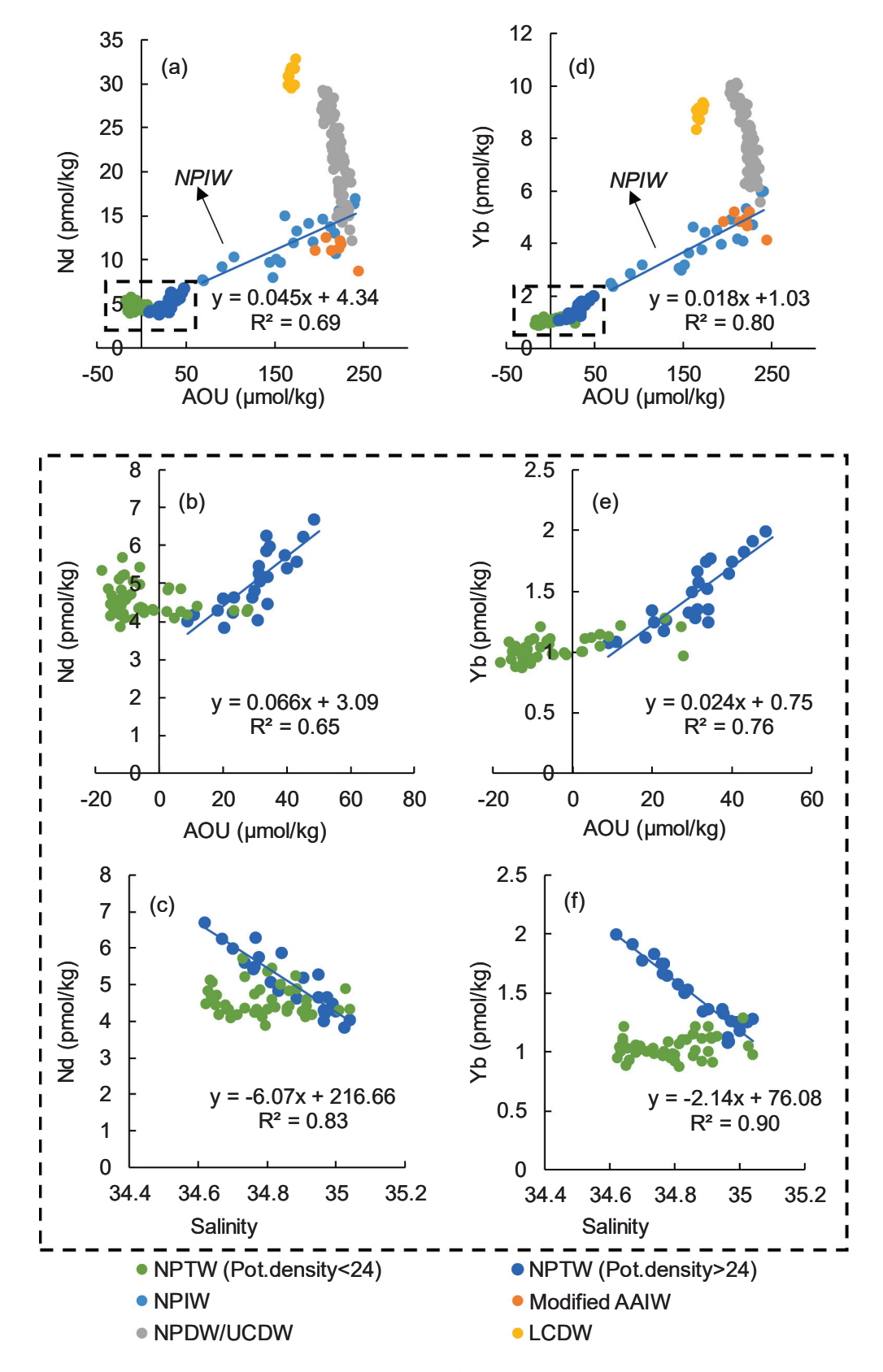


Fig. 8. (a) Nd (pmol/kg) vs. AOU ( $\mu$ mol/kg) and (d) Yb (pmol/kg) vs AOU ( $\mu$ mol/kg) for all samples within NPTW, NPIW, modified AAIW, NPDW/UCDW mixed water, and LCDW. The linear regression curves (solid lines) and fitting equations within NPIW are shown in (a) and (d). Both Nd and Yb are significantly positively correlated with AOU (P < 0.01). Inset dashed boxes in panels (a) and (d) are expanded to (b), (c), (e), and (f), which show (b) Nd vs. AOU, (c) Nd vs. salinity, (e) Yb vs. AOU, (f) Nd vs. salinity within NPTW. The  $\sigma_0 = 24$  kg/m³ isopycnal lies near 160 m, below the depth of chlorophyll maxima (DCM). The linear regression curves (solid lines) and equations within NPTW (>160 m) are shown.

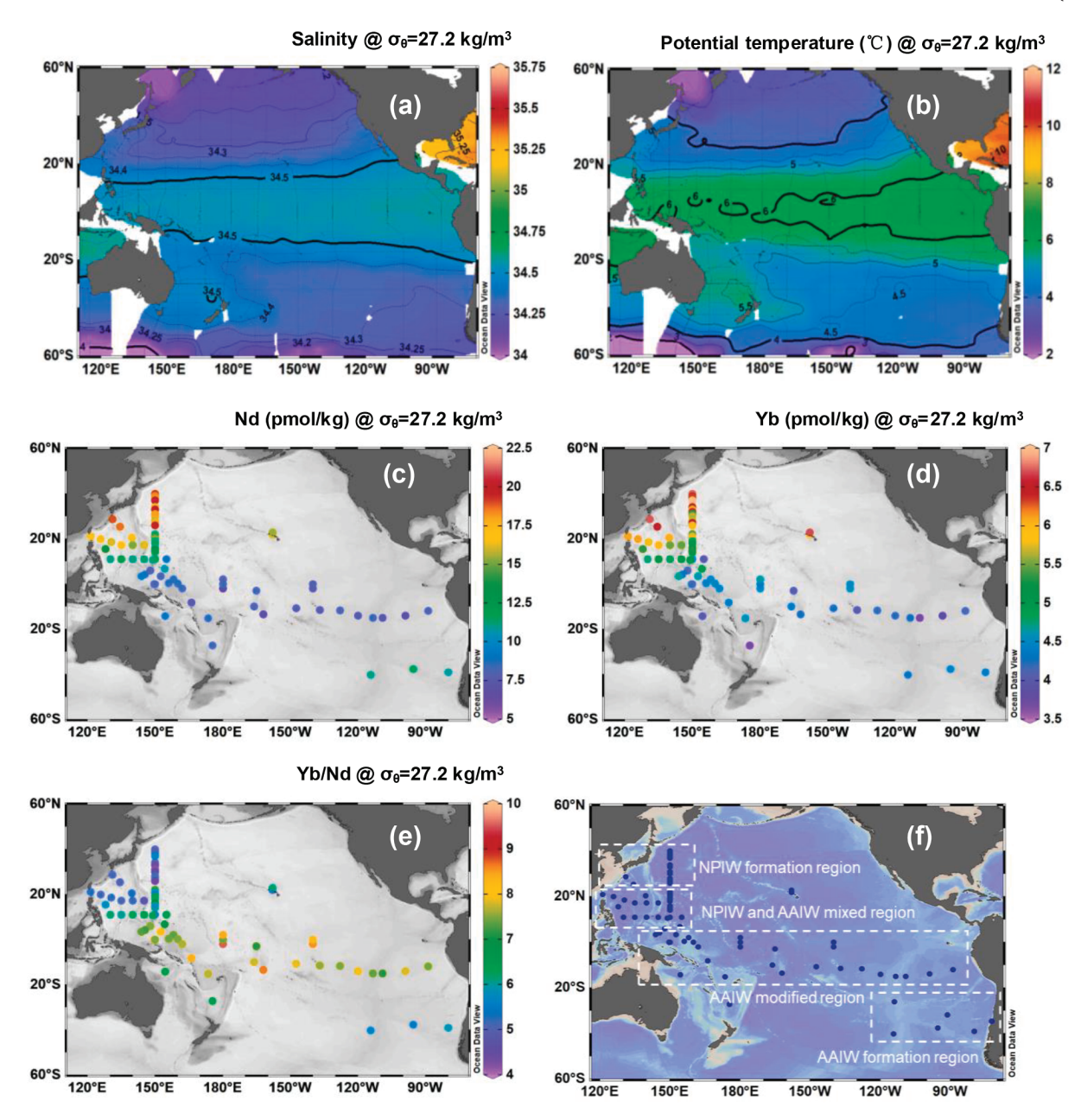


Fig. 9. Distributions of (a) salinity, (b) potential temperature (°C), (c) Nd (pmol/kg), (d) Yb (pmol/kg), and (e) Yb/Nd ratio at  $\sigma_\theta = 27.2$  kg/m³. (f) Map showing sampling stations (data from this study, Zhang and Nozaki (1996), Jeandel et al. (2013), Grenier et al. (2013), Fröllje et al. (2016), Molina-Kescher et al. (2014,2018), Behrens et al. (2018b), Haley et al. (2021), and Cao et al. (2023)) and the four sub-regions, which are NPIW formation region, AAIW modified region, and the NPIW and AAIW mixed region.

et al., 2010), AAIW modified region (S = 34.5  $\sim$  34.6, Bostock et al., 2010), and the NPIW and modified AAIW mixed region. To clarify the evolution of REEs along with water mass transport in the intermediate water, we compiled our REE data and published REE data in the Pacific (spanning from 40°N to 40°S, covering the northwest to southeast Pacific; Zhang and Nozaki, 1996; Jeandel et al., 2013; Grenier et al., 2013; Fröllje et al., 2016; Molina-Kescher et al., 2014, 2018; Behrens et al., 2018b; Haley et al., 2021; Cao et al., 2023). The lowest concentrations of REEs (Nd = 8.1  $\pm$  0.6 pmol/kg, Yb = 4.3  $\pm$  0.2 pmol/kg) and the highest Yb/Nd ratios (7.7  $\pm$  0.6) were found in the modified AAIW region, implying preferential removal of LREEs during AAIW transport from the Southeast Pacific to the equator (Figs. 9 and 10). The NPIW has the highest REE concentration (Nd = 18.4  $\pm$  1.2 pmol/kg, Yb = 6.3  $\pm$  0.3 pmol/kg; Figs. 9 and 10), reflecting a supply from the Subarctic Pacific surface water rich in lithogenic materials (Cao et al., 2023). These

observations indicate that different water masses carry distinct REE signatures.

In our study area, at a potential density of 27.2 kg/m³, the REE concentrations (Nd =  $13.6 \pm 2.6$  pmol/kg, Yb =  $5.2 \pm 0.6$  pmol/kg) fall within the range of REE end-members found in the NPIW and modified AAIW (Figs. 9 and 10). The Nd and Yb concentrations, as well as Yb/Nd ratios, strongly correlated with salinity (P < 0.01) with correlation coefficients of 0.90, 0.82, and 0.67, respectively. This suggests that the distributions of REE concentrations and composition at a potential density of 27.2 kg/m³ in the study area ( $10^{\circ}N-20^{\circ}N$ ) are primarily controlled by the mixing NPIW and modified AAIW. This is generally consistent with previous physical oceanographic observations of AAIW intruding northward to  $10-15^{\circ}N$  (Wang et al., 2015; Zang et al., 2020). REEs can serve as reliable indicators of water mass mixing, although it's worth noting that the remineralization process generally also

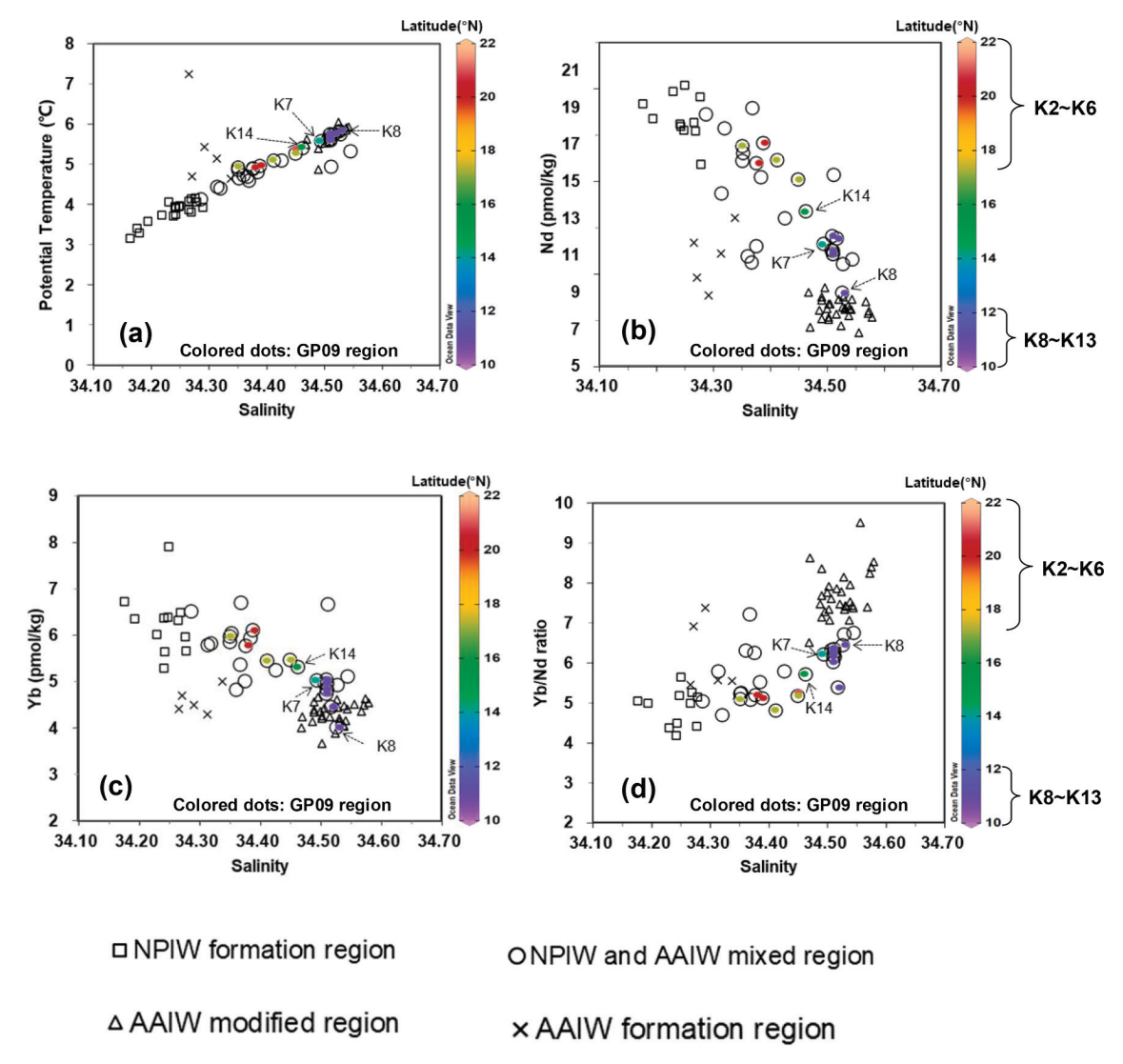


Fig. 10. (a) Potential temperature (°C) vs. salinity, (b) Nd (pmol/kg) vs. salinity, (c) Yb (pmol/kg) vs. salinity, and (d) Yb/Nd ratio vs. salinity for all samples within the four sub-regions. The color represents the latitudes of stations from GP09. Data from this study, Zhang and Nozaki (1996), Jeandel et al. (2013), Grenier et al. (2013), Fröllje et al. (2016), Molina-Kescher et al. (2014,2018), Behrens et al. (2018b), Haley et al. (2021), and Cao et al. (2023).

contributes to the REEs in intermediate water (Stichel et al., 2015; Lambelet et al., 2016; Behrens et al., 2018a,b). To quantitatively assess the semi-conservative behavior of REEs, an analysis of the mixing ratios of intermediate waters in the study area were conducted, as elaborated in section 4.3.3.

In the eastern equatorial Pacific, evidence of Nd scavenging in intermediate water was linked to the region's high productivity (Grasse et al., 2012; Molina-Kescher et al., 2014). Intense particle export rates would remove large amounts of dissolved Nd, leading to low REE concentrations. Behrens et al., (2018b) proposed that the low Nd concentration in the modified AAIW in the West Pacific ( $10.6^{\circ}N \sim 15^{\circ}S$ ) near the equator was due to extensive scavenging occurring in the Southern Ocean opal belt. At approximately11°N (stations K8-K13), low REE concentrations (Nd =  $11.1 \pm 1.1$  pmol/kg, Yb =  $4.7 \pm 0.4$  pmol/kg; Fig. 9c and d) and high Yb/Nd ratios (6.1  $\pm$  0.4) were observed (Fig. 9e), which were close to the modified AAIW at the equator. Therefore, it is suggested that the low REE concentrations and high Yb/Nd ratios at ~ 11°N are primarily supplied by the modified AAIW. Fig. 10 shows that station K8 exhibited the most similar REE concentration and Yb/Nd ratio to modified AAIW compared to other stations during the GP09 cruise, signifying a stronger influence from the modified AAIW water mass. This observation is consistent with the westward flow of modified AAIW from the eastern Pacific around  $\sim 10^{\circ}$ N, as reported by Kawabe et al. (2010). The removal of Nd in intermediate water was also observed in the north of the Solomon Sea (stations 30 and 24, Grenier et al., 2013) with a salinity (34.49 to 34.52) similar to that of modified AAIW. This may be explained by the supply of modified AAIW from the eastern equatorial Pacific.

The low Nd concentration in the modified AAIW in the West Pacific  $(10.6^{\circ} N \sim 15^{\circ} S)$  (Behrens et al., 2018b) was lower compared to that in the AAIW formation region in the Southwest Ocean, and the Yb/Nd ratio was higher (Figs. 9 and 10). This suggests that the removal of REEs also occurs during AAIW transport from the formation region to near the equator, not solely in the opal belt region of the Southern Ocean. It may be related to the high export of particulate matter from the highly productive region of the eastern Pacific.

4.3.3. Semi-conservative behavior of HREEs and non-conservative addition of LREEs in the water layer at  $27.2 \text{ kg/m}^3$ 

As elucidated in section 4.3.2, REE concentrations in the intermediate water were primarily influenced by the prevailing water masses within this study area, with noticeable REEs scavenging observed at the equatorial and southern latitudes. Accordingly, the core focus of this study was on assessing the applicability of REEs as tracers for water

masses and their specific semi-conservative behavior within the NPIW and modified AAIW mixed region.

The fraction of modified AAIW in the study area, as depicted in Fig. 11a, was predominantly concentrated south of 11°N (~100 %), generally consistent with the physical oceanographic observations by Kawabe and Fujio (2010) and Wang et al. (2015). The percentages of non-conservative Nd and Yb in the total concentration (ΔNd/Nd and  $\Delta Yb/Yb)$  ranged from 14 % to 31 % (average 25 %  $\pm$  5 %) and from -3% to 12 % (average 7 %  $\pm$  4 %), respectively (Fig. 11c and d). Considering the relative standard deviation in REEs analysis (mostly less than 5 %) and potential errors introduced by the two end-members mixing model, we regard the addition of Nd as significant, while the addition or removal of Yb as negligible. This implies that Nd exhibits non-conservative behavior, whereas Yb displays semi-conservative characteristics during transport along the isopycnic surface of 27.2 kg/m<sup>3</sup>. HREEs can serve as novel tracers for quantifying mixing ratios of water masses at the basin scale. In prior studies, apart from conventional oceanographic tracers (potential temperature and salinity), most chemical tracers employed to track large-scale ocean circulation relied on isotopes (e.g.,  $\Delta^{14}$ C, Nd isotopes, and Ra isotopes) (Lacan and Jeandel, 2001; Bostock et al., 2013; Xu et al., 2022). High-resolution tracer data is crucial for advancing our understanding of global ocean circulation. The potential of REE concentrations to provide higherresolution sampling, owing to their minimal measurement volume requirements and cost-effectiveness of measurement, positions them as significantly valuable tools for enriching our comprehension of ocean circulation. In regions with numerous water masses, such as east of Taiwan Island, where contributions from modified AAIW, NPIW, intermediate water from the South China Sea, and vertical mixing due to a densely-packed eddy field are expected, relying solely on temperature and salinity may not quantify the mixing. In such cases, HREEs may serve as potential semi-tracers for the identification and quantification of water masses, drawing upon the framework established in Zhang et al. (2018) and Liu et al. (2022). In addition to  $\Delta Nd$ , we also estimated the excess nitrate ( $\Delta N$ ) and excess phosphate ( $\Delta P$ ). Both  $\Delta N$  and  $\Delta P$ exhibited a significant positive correlation with AOU (R<sup>2</sup> = 0.82, P < 0.01 for  $\Delta N$ ;  $R^2 = 0.73$ , P < 0.01 for  $\Delta P$ ), providing evidence of remineralization processes occurring within the water layer at 27.2 kg/m<sup>3</sup>. Nevertheless, no correlation was observed between  $\Delta Nd$  and AOU (Fig. 11b), indicating that the excess Nd is not solely contributed by remineralization processes. The potential source of the excess Nd will be discussed in section 4.4.1.

## 4.4. Conservative versus non-conservative processes for REEs in deep water

### 4.4.1. Potential REE sources from slope sediments

Dissolved Ce is very easily oxidized and scavenged in the ocean, therefore negative Ce anomalies are generally observed in seawater, becoming more negative with water depth (de Baar et al., 1988, 2018).

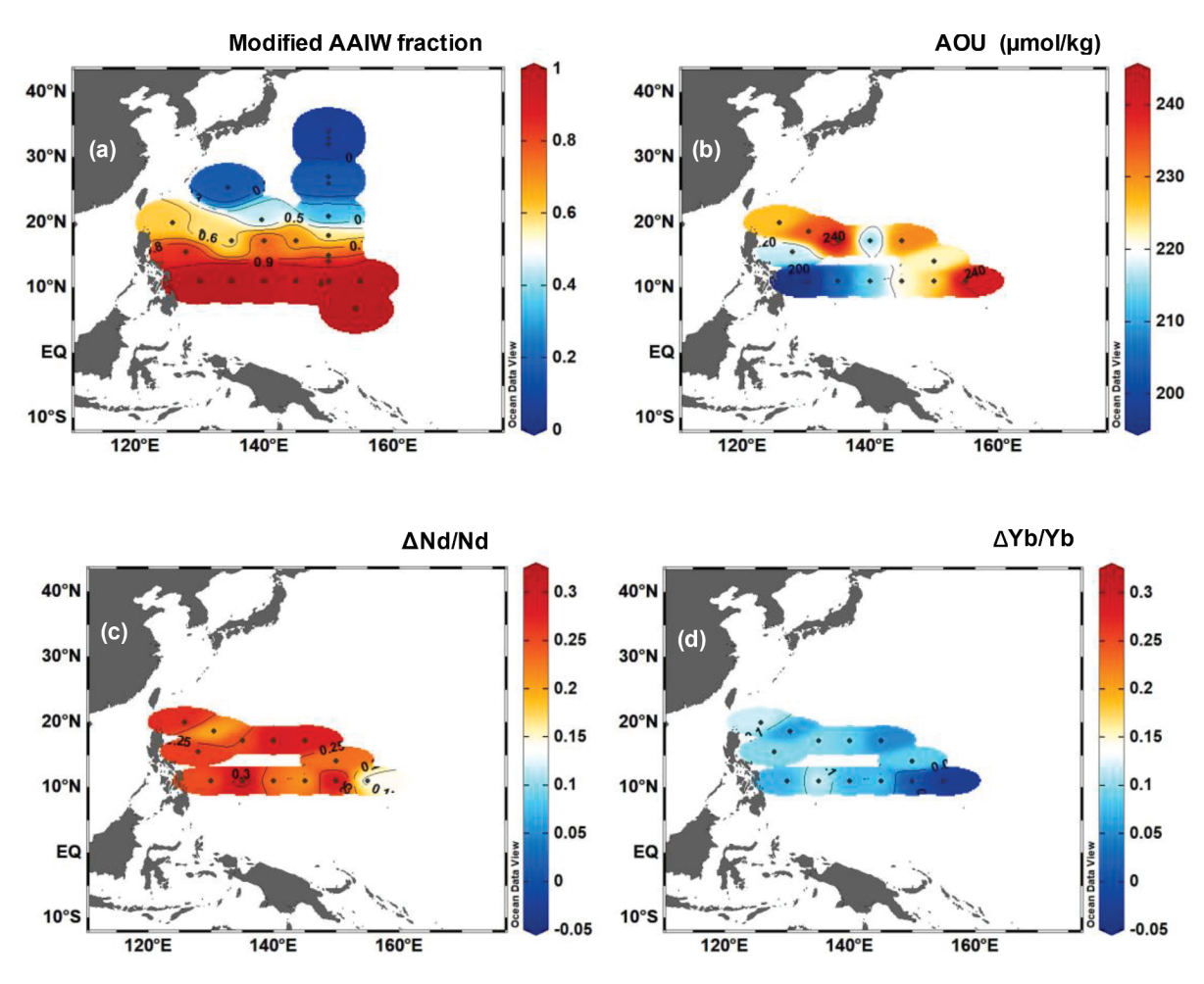


Fig. 11. Map showing (a) the calculated modified AAIW fraction, where "1" means that 100 % of the seawater is sourced from the modified AAIW, (b) AOU ( $\mu$ mol/kg), (c)  $\Delta$ Nd/Nd, and (d)  $\Delta$ Yb/Yb at  $\sigma_{\theta} = 27.2$  kg/m³. The  $\Delta$ Nd/Nd and  $\Delta$ Yb/Yb represent the Nd and Yb addition/removal (i.e. the difference between observed concentrations and concentrations calculated from simple mixing of the end-members) relative to the observed Nd and Yb concentrations, respectively.  $\Delta$ Nd/Nd or  $\Delta$ Yb/Yb close to 0 indicates that Nd or Yb is behaving conservatively. Positive values indicate the addition of Nd or Yb. Negative values indicate the removal of Nd or Yb. The addition or removal of Nd and Yb originates from non-conservative processes along the path from the endmember region we defined to the study area.

However, deep water (below 1500 m) at station K1 exhibited less negative Ce/Ce\* values compared to the rest of the section in the same depth range (Fig. 7). These waters also showed low Yb/Nd values (<5) (Fig. 6a and c). This can be explained by the input of lithogenic material from slope sediments, as lithogenic particles typically do not have significant negative Ce anomalies or fractionation between LREEs and HREEs compared to the composition of REEs in seawater (Pearce et al., 2013; Garcia-Solsona et al., 2014; Paffrath et al., 2021). The presence of suspended particles in the deep water (>1500 m) at station K1, as indicated by low beam transmission (Supplementary Fig. S9), further supports the input from suspended particles. Besides, less negative values of Ce/Ce\* at ~800 m in stations K12, K13, and K14 (Fig. 7) with no decline in beam transmission were speculated to be affected by the lateral transport by the persistent anticyclonic eddy in this layer (Supplementary Fig. S4; Wang et al., 2016; Zhang et al., 2021). These values are likely imprinted by slope sediments originating from the Philippine Islands. As mentioned in section 4.3.3, an addition of nearly 31 % Nd was observed at stations K12, K13, and K14 at a density of 27.2 kg/m<sup>3</sup> (corresponding to water depths of 740 m, 670 m, and 740 m, respectively). This additional input could be partly attributed to the Philippine Islands, supported by the weak Ce anomalies observed in this area.

During the cruise, elevated concentrations of dissolved Fe were observed at  ${\sim}800$  m water depth in stations K12, K13 and K14 (0.8  $\pm$  0.1 nmol/kg), which were 36 % higher than those at similar depths in stations located further from the island (stations K8 to K11). The dissolved REEs and Fe derived from lithogenic sources have been found in seawater near the PNG Islands and the Kerguelen Plateau in the Southern Ocean (Sholkovitz et al., 1999; Zhang et al., 2008). Therefore, we suggest that the combination of less negative Ce anomalies and elevated Fe concentrations at stations K12/K13/K14 ( ${\sim}800$  m) is indicative of a potential source from slope sediments and water mass transport.

### 4.4.2. Modifications of REE in seawater by hydrothermal fluids

In this study area, a number of active volcanoes and hydrothermal vents are located in the Mariana Trough around 143.5° to 144.9° E and  $12.8^{\circ}$  to  $18.2^{\circ}$  N. These vents have depths ranging from 2880 m to 4192 m (Supplementary Fig. S10) (https://vents-data.interridge.org/). High concentrations of dissolved Fe were observed at depths of 2500  $\sim$  3400 m at station K6 (2.3  $\pm$  0.3 nmol/kg), implying the presence of hydrothermal activity. Eu anomalies are often associated with hydrothermal activity, as Eu exists primarily in the reduced state Eu<sup>2+</sup> in hightemperature hydrothermal fluids. The decreased adsorption strength of Eu<sup>2+</sup> to particles in the fluid leads to a relatively higher concentration of Eu and a positive Eu anomaly in the fluid (Michard et al., 1983; Sverjensky, 1984; Michard, 1989). Positive Eu anomalies due to hydrothermal fluid mixing have been found in the North Atlantic Ocean and Central Arctic Ocean (Stichel et al., 2018; Paffrath et al., 2021). However, no significant Eu anomalies or altered REE concentrations were observed in our study area (Fig. 3; Supplementary Fig. S11). Two possible explanations can be considered. Firstly, some Fe in hydrothermal fluids, such as in the form of organic complexes, may be protected from scavenging processes, leading to its stability in seawater (Bennett et al., 2008; Wu et al., 2011; Yücel et al., 2011), while REEs in the fluid and surrounding seawater may be rapidly scavenged by Fe-Mn oxides present around the vents (German et al., 1991; Rudnicki and Elderfield, 1993; Mitra et al., 1994; Zheng et al., 2016; Stichel et al., 2018; Chavagnac et al., 2018). However, no significant removal of REEs was observed at the bottom of station K6 (Figs. 3 and 5), and thus it can be ruled out that Fe-Mn oxides influence REEs in this hydrothermal zone. Secondly, we propose that the input of REEs from the weak hydrothermal activity in our study area is not significant. The continuous dilution of seawater may prevent the small flux of REE inputs from hydrothermal fluid from causing a noticeable increase in REE concentrations in the surrounding seawater. Although further investigation is required to confirm this hypothesis, our findings suggest that in cases of weak hydrothermal activity, the Eu anomalies in seawater may not be significantly positive, and the input flux of REEs from hydrothermal fluids at the sampling site may be negligible.

Additionally, high Yb/Nd ratios were found significant in 800-2000 m of water at  $11^{\circ}$ N (Fig. 6a and c). The upper samples (~800 m), which include AAIW affected by the opal belt in the Southern Ocean and the eastern equatorial high productivity area were discussed in section 4.3. REEs in deeper waters (UCDW,  $\sim$ 1500 m) appear to be influenced by the intense scavenging by Fe-Mn oxides formed in hydrothermal plumes near the Solomon Islands and Tonga-Fiji region (Lupton et al., 2004, 2015; Behrens et al., 2018b), resulting in elevated Yb/Nd ratio. The high helium isotope plume at 1500 m water depth could clarify the hydrothermal activity near the Solomon Islands and Tonga-Fiji region (Supplementary Fig. S12). In addition, the low Dy/Er ratio is speculated to be caused by hydrothermal activity, since the plume of East Pacific Rise showed a low Dy/Er ratio while the particle samples from the hydrothermal pool had a relatively high Dy/Er ratio (Klinkhammer et al., 1983; Sherrell et al., 1999; Osborne et al., 2015). The low Dy/Er ratio (<0.6) we found in 1000-2000 m water may also indicate that the REE patterns in the study area is influenced by the vent field (Fig. 6b and d).

# 4.4.3. Semi-conservative behavior and non-conservative processes for REEs in deep water (>2000 m)

In the deep water (>2000 m), the REEs exhibited an increase either independently of AOU (LCDW) or while AOU was decreasing (NPDW/ UCDW) (Fig. 8a and d). This pattern indicates that remineralization processes were not the dominant factor affecting dissolved REEs in deep water. The concentrations of REEs remained relatively constant below 4000 m, with a slight decrease observed at the bottom layer in stations K7, K8, and K9 (Eastern Marianas Basin) (Figs. 3 and 5), possibly influenced by the presence of LCDW with low REE concentrations (Station GeoB17014; Nd =  $32.2 \pm 1.0$  pmol/kg, Yb =  $9.8 \pm 0.1$  pmol/ kg; Behrens et al., 2018b). Specifically, at station K7 (bottom depth = 6033 m), the transmission decreased from 101.4 % at 5300 m to 101.2 % at 5940 m (Supplementary Fig. S9), supporting the presence of resuspended particulate matter. This implies that the very slight decrease in concentration in deep water at station K7 (>5000 m, Nd = 31.1  $\pm$  0.7 pmol/kg, Yb =  $9.1 \pm 0.1$  pmol/kg) resulted from a combination of particulate scavenging and lateral transport from the LCDW. However, at station K8 (Nd = 29.7  $\pm$  0.3 pmol/kg, Yb = 8.5  $\pm$  0.3 pmol/kg), the scavenging of REEs in deep water by suspended particles can be excluded because the benthic nepheloid layers were absent (Supplementary Fig. S9; Gardner et al., 2018). Possible reasons for the low concentrations will be interpreted below. The REE concentrations in LCDW (>4500 m) in the Philippine Basin and West Mariana Basin (stations K2, K3, K5, K11, K13, and K14; Nd = 33.8  $\pm$  2.0 pmol/kg, Yb =  $10.1 \pm 0.3$  pmol/kg) were similar to those in the Tropical Pacific (154.2°E, 6.8°N; Station GeoB17014; Behrens et al., 2018b). This reflects that the REE concentrations, especially HREEs, were nearly conservative with LCDW transport from the tropics to the subtropical Western Marianas Basin and Philippine Basin. At station K1, the presence of a weaker Ce negative anomaly and low transmission below 1500 m indicated a particulate source of REEs (section 4.4.1). Meanwhile, the Pacific deep water sinks at 1500 m in the Luzon Strait and enters the South China Sea (Xu and Oey, 2014). Therefore, REEs in deep water at station K1 should be influenced by both particulate matter input and water mass flow.

To quantify the fractions of conservative and non-conservative behaviors for REE in deep water, we estimated the mixing ratios of three water masses (NPDW, UCDW, and LCDW) at water depths >2000 m using potential temperature and salinity (Eqs. (1)–(3)).  $\Delta$ Nd and  $\Delta$ Yb were calculated as the difference between the observed concentration and the concentration resulting from the water mass mixing. The results are shown in Fig. 12. The UCDW, with low end-member values of REEs, were distributed in deep water in station K1 (<2100 m) with a fraction of more than 70 %. The fraction of LCDW was more than 50 % below

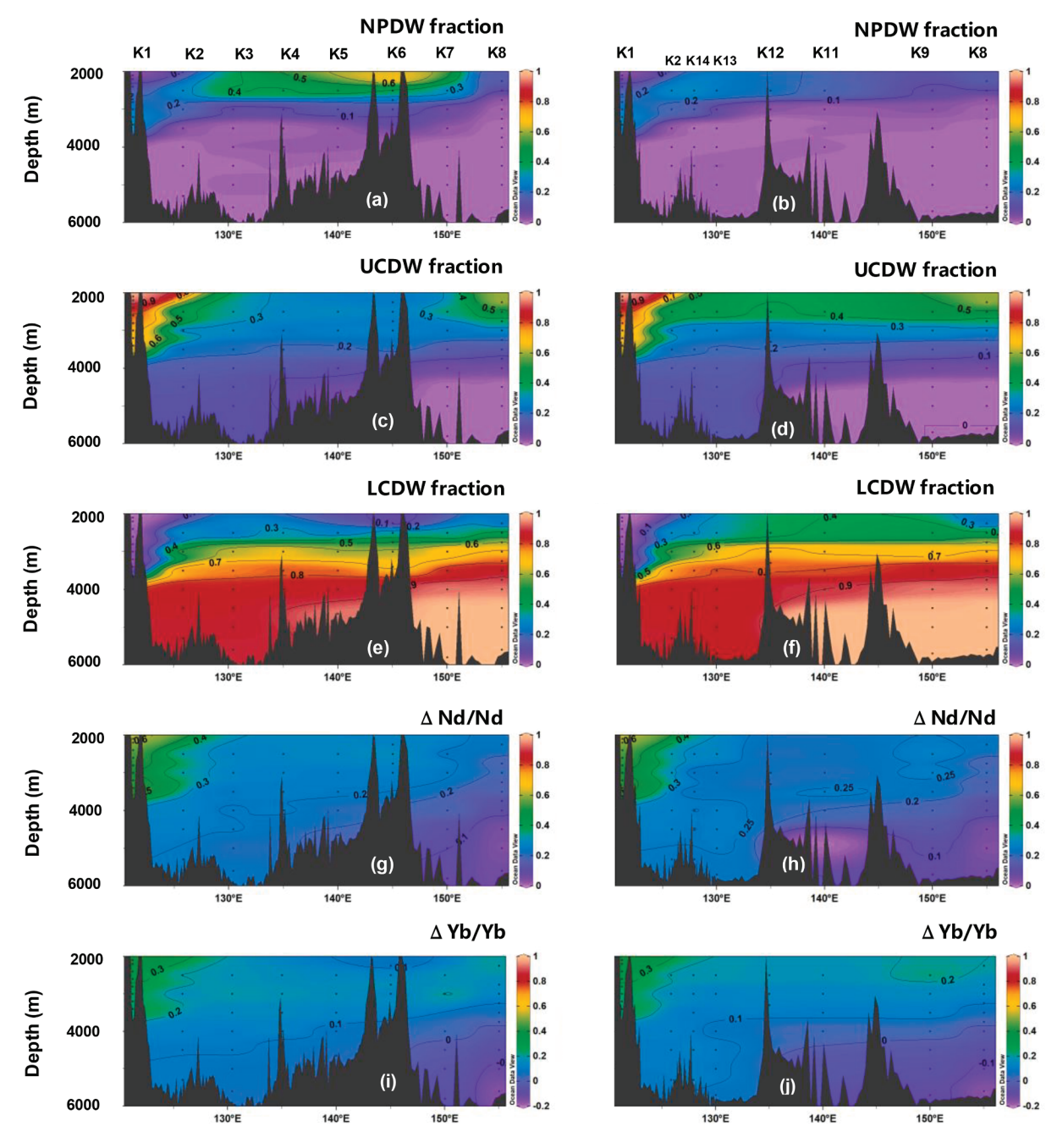


Fig. 12. Calculated (a, b) mixing factions of NPDW, (c, d) UCDW, (e, f) LCDW, (g, h)  $\Delta$ Nd/Nd and (i, j)  $\Delta$ Yb/Yb along transects N (left panels) and S (right panels).

3500 m, which is in general agreement with the results reported by Behrens et al. (2018b) in the West Pacific. Notably, the fraction of LCDW below 4500 m at stations K7, K8, and K9 (East Mariana Basin) is approximately 100 % and decreases at western stations (stations K2, K3, K13, K14). This result indicates that LCDW was flowing from the East Mariana Basin to the West Mariana Basin. Our calculations align with water mass pathways models in the deep ocean (Qu et al., 2006; Kawabe et al., 2003, 2009; Kawabe and Fujio, 2010). The above-mentioned supported the reliability of our estimated results.

As shown in Fig. 12g  $\sim$  j, in the Luzon Strait (station K1), elevated  $\Delta Nd/Nd$  (48–63%) and  $\Delta Yb/Yb$  (27–40%) values indicated an input of external material. This observation is consistent with the less negative Ce anomalies below 1500 m, confirming a contribution from particle sources of dissolved REEs. In other stations, except for station K1, the  $\Delta Nd/Nd$  and  $\Delta Yb/Yb$  values ranged from 0  $\sim$  30% and  $-16 \sim$  20%,

respectively. Excess Yb ( $\Delta$ Yb) strongly positively correlated with AOU at water depths > 2000 m (n = 69, R² = 0.70, P < 0.01), reflecting the contribution of organic matter remineralization to excess HREEs. From the same cruise data, we observed a significant positive correlation between excess Yb ( $\Delta$ Yb) and silicate (figure not shown, n = 69, R² = 0.55, P < 0.01). However, the maximum  $\Delta$ Yb was not located in the bottom water (Fig. 12i and j). This suggests that excess HREEs may originate from the remineralization and dissolution of particles, including organic particles and siliceous particles, during sinking in the deep water (>2000 m), rather than benthic input from the seafloor. Akagi et al. (2011) also reported that the dissolution of siliceous particulate matter is an important source of REEs in the deep North Pacific Ocean. In contrast, no significant correlations were observed between excess Nd ( $\Delta$ Nd) and AOU, or between  $\Delta$ Nd and silicate, which means the complex behavior of LREEs in seawater. This arises from the weaker

complexation of LREEs by inorganic ligands in solution compared to HREEs (Goldberg et al., 1963), rendering them more susceptible to adsorption by particulate matter. A previous study reported that dissolved LREEs in deep water were associated with the scavenging of carbonate/oxides (Akagi, 2013). Schijf et al. (2015) estimated that hydrated manganese oxide (HMO) is the dominant scavenger of REEs in Pacific deep water using a scavenging model. The scavenging and release from particles may be responsible for the complex behavior of LREEs observed in our study and need to be further investigated.

As shown in Fig. 12, there is a small amount of Yb removal ( $\Delta$ Yb/Yb =-16 %) and approximately conservative behavior of Nd ( $\Delta$ Nd/Nd =6%) in the deep water (5600 m) at station K8 (bottom depth = 5717 m), which suggests the potential presence of a sink for seawater HREEs. There is a large spatial difference in the REE concentrations of the porewater in the northwest Pacific basin. For instance, the total REE concentrations (from La to Yb) in the upper porewater (0-3 cm) is 3198 pmol/kg in the Pigafetta Basin (station MABC25, near 20°N and 160°E) (Deng et al., 2017), while it is only 117 pmol/kg near the Kyushu-Palau Ridge (stations XTZZ40 and XTZZb4, near 15°N and 135°E) (Che et al., 2020) (Supplementary Fig. S13). According to the REE concentrations in porewater reported by Che et al. (2020), it can be seen that the Yb concentration in porewater near the Kyushu-Palau Ridge is much lower than that in deep seawater (5600 m) at station K8. Therefore, we speculate that the small decrease of HREEs in the deep water at station K8 may be associated with the dilution effect of low-concentration

Behrens et al. (2018b) suggested that in the open ocean near South Korea and the Tropical West Pacific, the distribution of HREEs in deep water is dominantly controlled by water masses rather than benthic sources or particle release. Our calculations in the northwest Pacific also support this finding, showing that water masses have a major control over the distribution of HREEs (>80 % for Yb) in deep water (>2000 m). Furthermore, even though non-conservative processes have a minor contribution to HREEs (<20 % for Yb), we illustrate, through the distribution of the maximum  $\Delta Yb$  and their correlation with AOU and silicate, that the excess HREEs were attributed to the release of sinking particles.

### 5. Conclusions

In this study, we conducted an extensive investigation into the sources and distribution of REEs in the seawater of the NPSG using high-resolution seawater sampling collected during the GEOTRACES GP09 cruise. We aimed to unravel the controlling factors of REEs throughout the water columns and trace the sources and water mass transport through the fractionation patterns of REEs. The key conclusions of this study are summarized as follows:

- (1) Surface waters along ~11°N showed slightly elevated REE concentrations (Nd = 6.1  $\pm$  1.0 pmol/kg, Yb = 1.3  $\pm$  0.2 pmol/kg) and significant Eu positive anomalies (Eu/Eu\* = 1.3  $\pm$  0.1), which were attributed to the input of lithologic materials from volcanic islands such as the Philippine and Hawaii Islands.
- (2) In the intermediate water layer (at a potential density of 27.2 kg/m³), distinct REE concentrations and ratio characteristics were observed in different regions of the Pacific Ocean. NPIW displayed high REE concentrations due to lithogenic sources, while modified AAIW exhibited low REE concentrations and high Yb/Nd ratios, resulting from particle scavenging processes. In this study area, the REE concentrations and Yb/Nd ratios served as tracers for the mixing of NPIW and modified AAIW. By estimating the mixing ratio of intermediate water, we found that HREEs are predominantly controlled by water mass mixing (93 % ± 4% for Yb) and demonstrated the utility of HREEs as tracers for intermediate water mixing in the northwest Pacific.

- (3) Less negative Ce anomalies in deep water (>1500 m) at Luzon Strait (station K1) and intermediate water (~800 m) near Philippine islands (stations K12, K13, and K14) indicated the release of particles or sediments from the islands slope. A significant addition of approximately 31 % Nd at ~800 m near the Philippine islands also suggested a partial contribution from island input.
- (4) Over 80 % of the Yb (a representative for HREEs) and 70 % of the Nd (a representative for LREEs) in deep waters (>2000 m) in the study area (excluding station K1) were contributed by deep water mass mixing (NPDW, UCDW, and LCDW). The non-conservative behavior of HREEs (<20 % for Yb) was primarily associated with the release by sinking particles (organic and siliceous particles). This conclusion is supported by the absence of maximum ΔYb concentration in bottom water and the presence of significant positive correlations between  $\Delta Yb$  and AOU as well as  $\Delta Yb$ and Si. The non-conservative behavior of LREE (<30 % for Nd) may be influenced by a combination of particle release and scavenging processes, requiring further investigation. Combining high-resolution REE measurements with water mass analysis allows for a quantitative assessment of the interplay between physical and biogeochemical processes in the REEs cycling, which have not been previously documented and cannot be recognized by REE concentrations and composition alone.

In summary, this study enhances our understanding of REE cycling in the northwest Pacific, particularly regarding lithogenic sources and biogeochemical processes. It also underscores the significant potential of HREEs as tracers for basin-scale water mass mixing, providing valuable insights into ocean circulation.

### CRediT authorship contribution statement

Axiang Cao: Writing – original draft, Visualization, Investigation, Formal analysis, Data curation, Conceptualization. Qian Liu: Writing – review & editing, Supervision, Project administration, Investigation, Conceptualization. Jing Zhang: Writing – review & editing, Supervision, Project administration, Conceptualization. Alan M. Shiller: Project administration, Data curation. Yihua Cai: Writing – review & editing, Investigation, Data curation. Ruifeng Zhang: Writing – review & editing, Investigation. Melissa Gilbert: Data curation. Xianghui Guo: Writing – review & editing, Data curation. Zhiyu Liu: Writing – review & editing, Visualization.

### Declaration of competing interest

The authors declare that they have no known competing financial interests or personal relationships that could have appeared to influence the work reported in this paper.

### Acknowledgments

We thank the captain and crew of the R/V TAN KAH KEE for their help with sampling. We further thank Dr. Hongyang Lin and Zhendong Hu from Xiamen University for providing the results of the oceanic current field. We also thank Siteng Zhu from the University of Toyama for help with the model calculation and Li Ma and Xianxian Wang from the Ocean University of China for their help in the clean laboratory. Special thanks to Dr. Huijun He for his important guidance during the experiment and early writing stage. Hydrographic data from cruise GP09 used in this publication came from the State Key Laboratory of Marine Environmental Science (Xiamen University). We thank editors Drs. Tim M. Conway and Jeffrey G. Catalano, and two anonymous reviewers for their constructive reviews, which significantly improve this manuscript. This research was supported by the National Natural Science Foundation of China (Grant 41890801), National Key Research and

Developmental Program of China (Grant 2023YFF0805001), JSPS KAKENHI (Grants JP20H04319, JP22H05206), and US National Science Foundation (Grant OCE 1925503).

### Appendix A. Supplementary material

The supplemental file includes information related to the data of hydrographic parameters and REEs in the study area and flow field maps, etc. Supplementary material to this article can be found online at https://doi.org/10.1016/j.gca.2024.02.018.

#### References

- Akagi, T., 2013. Rare earth element (REE)-silicic acid complexes in seawater to explain the incorporation of REEs in opal and the "leftover" REEs in surface water: new interpretation of dissolved REE distribution profiles. Geochim. Cosmochim. Acta 113, 174–192.
- Akagi, T., Fu, F., Hongo, Y., Takahashi, K., 2011. Composition of rare earth elements in settling particles collected in the highly productive North Pacific Ocean and the Bering Sea: Implications for siliceous-matter dissolution kinetics and formation of two REE-enriched phases. Geochim. Cosmochim. Acta 75, 4857–4876.
- Amakawa, H., Alibo, D.S., Nozaki, Y., 2004. Nd concentration and isotopic composition distributions in surface waters of Northwest Pacific Ocean and its adjacent seas. Geochem. J. 38, 493–504.
- Behrens, M.K., Pahnke, K., Schnetger, B., Brumsack, H.-J., 2018a. Sources and processes affecting the distribution of dissolved Nd isotopes and concentrations in the West Pacific. Geochim. Cosmochim. Acta 222, 508–534.
- Behrens, M.K., Pahnke, K., Paffrath, R., Schnetger, B., Brumsack, H.-J., 2018b. Rare earth element distributions in the West Pacific: trace element sources and conservative vs. non-conservative behavior. Earth Planet. Sci. Lett. 486, 166–177.
- Behrens, M.K., Pahnke, K., Cravatte, S., Marin, F., Jeandel, C., 2020. Rare earth element input and transport in the near-surface zonal current system of the Tropical Western Pacific. Earth Planet. Sci. Lett. 549, 116496.
- Bennett, S.A., Achterberg, E.P., Connelly, D.P., Statham, P.J., Fones, G.R., German, C.R., 2008. The distribution and stabilisation of dissolved Fe in deep-sea hydrothermal plumes. Earth Planet. Sci. Lett. 270, 157–167.
- Bostock, H.C., Opdyke, B.N., Williams, M.J.M., 2010. Characterising the intermediate depth waters of the Pacific Ocean using  $\delta$ 13C and other geochemical tracers. Deep Sea Res. Part I Oceanogr. Res. Pap. 57, 847–859.
- Bostock, H.C., Sutton, P.J., Williams, M.J.M., Opdyke, B.N., 2013. Reviewing the circulation and mixing of Antarctic Intermediate Water in the South Pacific using evidence from geochemical tracers and Argo float trajectories. Deep Sea Res. Part I: Oceanogr. Res. Pap. 73, 84–98.
- Bruland, K.W., 1980. Oceanographic distributions of cadmium, zinc, nickel, and copper in the North Pacific. Earth Planet. Sci. Lett. 47, 176–198.
- Cao, A., Zhang, J., Zhang, H., Chen, Z., Cui, G., Liu, Z., Li, Y., Liu, Q., 2023. Dissolved rare earth elements in the Northwest Pacific: sources, water mass tracing, and crossshelf fluxes. Front. Mar. Sci. 10, 1135113.
- Chavagnac, V., Saleban Ali, H., Jeandel, C., Leleu, T., Destrigneville, C., Castillo, A., Cotte, L., Waeles, M., Cathalot, C., Laes-Huon, A., Pelleter, E., Nonnotte, P., Sarradin, P.-M., Cannat, M., 2018. Sulfate minerals control dissolved rare earth element flux and Nd isotope signature of buoyant hydrothermal plume (EMSO-Azores, 37°N Mid-Atlantic Ridge). Chem. Geol. 499, 111–125.
- Che, H., Hu, B., Ding, X., Song, W., Guo, J., Cui, R., Deng, Y., 2020. Rare earth element geochemistry characteristics and implications of pore-water from deep sea sediment in Western Pacific Ocean. Mar. Geol. Quat. Geol. 41 (1), 75–86.
- Che, H., Zhang, J., 2018. Water Mass Analysis and End-Member Mixing Contribution Using Coupled Radiogenic Nd Isotopes and Nd Concentrations: Interaction Between Marginal Seas and the Northwestern Pacific. Geophys. Res. Lett. 45, 2388–2395.
- de Baar, H.J.W., German, C.R., Elderfield, H., van Gaans, P., 1988. Rare earth element distributions in anoxic waters of the Cariaco Trench. Geochim. Cosmochim. Acta 52, 1203–1219.
- de Baar, H.J.W., Bruland, K.W., Schijf, J., van Heuven, S.M.A.C., Behrens, M.K., 2018. Low cerium among the dissolved rare earth elements in the central North Pacific Ocean. Geochim. Cosmochim. Acta 236, 5–40.
- Deng, Y., Ren, J., Guo, Q., Cao, J., Wang, H., Liu, C., 2017. Rare earth element geochemistry characteristics of seawater and porewater from deep sea in western Pacific. Sci. Rep. 7. 16539.
- Fitzsimmons, J.N., Hayes, C.T., Al-Subiai, S.N., Zhang, R., Morton, P.L., Weisend, R.E., Ascani, F., Boyle, E.A., 2015. Daily to decadal variability of size-fractionated iron and iron-binding ligands at the Hawaii Ocean Time-series Station ALOHA. Geochim. Cosmochim. Acta 171, 303–324.
- Fröllje, H., Pahnke, K., Schnetger, B., Brumsack, H.-J., Dulai, H., Fitzsimmons, J.N., 2016. Hawaiian imprint on dissolved Nd and Ra isotopes and rare earth elements in the central North Pacific: local survey and seasonal variability. Geochim. Cosmochim. Acta 189, 110–131.
- Fuhr, M., Laukert, G., Yu, Y., Nürnberg, D., Frank, M., 2021. Tracing water mass mixing from the equatorial to the North Pacific Ocean with dissolved neodymium isotopes and concentrations. Front. Mar. Sci. 7, 603761.
- Garcia-Solsona, E., Jeandel, C., Labatut, M., Lacan, F., Vance, D., Chavagnac, V., Pradoux, C., 2014. Rare earth elements and Nd isotopes tracing water mass mixing

- and particle-seawater interactions in the SE Atlantic. Geochim. Cosmochim. Acta 125, 351–372.
- Garcia-Solsona, E., Pena, L.D., Paredes, E., Pérez-Asensio, J.N., Quirós-Collazos, L., Lirer, F., Cacho, I., 2020. Rare earth elements and Nd isotopes as tracers of modern ocean circulation in the central Mediterranean Sea. Prog. Oceanogr. 185, 102340.
- Gardner, W.D., Jo Richardson, M., Mishonov, A.V., Biscaye, P.E., 2018. Global comparison of benthic nepheloid layers based on 52 years of nephelometer and transmissometer measurements. Prog. Oceanogr. 168, 100–111.
- German, C.R., Campbell, A.C., Edmond, J.M., 1991. Hydrothermal scavenging at the Mid-Atlantic Ridge: Modification of trace element dissolved fluxes. Earth Planet. Sci. Lett. 107, 101–114.
- Goldberg, E.D., Koide, M., Schmitt, R.A., Smith, R.H., 1963. Rare-earth distributions in the marine environment. J. Geophys. Res. 68, 4209–4217.
- Grasse, P., Stichel, T., Stumpf, R., Stramma, L., Frank, M., 2012. The distribution of neodymium isotopes and concentrations in the Eastern Equatorial Pacific: water mass advection versus particle exchange. Earth Planet. Sci. Lett. 353–354, 198–207.
- Grenier, M., Jeandel, C., Lacan, F., Vance, D., Venchiarutti, C., Cros, A., Cravatte, S., 2013. From the subtropics to the central equatorial Pacific Ocean: neodymium isotopic composition and rare earth element concentration variations. J. Geophys. Res. Oceans 118, 592–618.
- Haley, B.A., Wu, Y., Muratli, J.M., Basak, C., Pena, L.D., Goldstein, S.L., 2021. Rare earth element and neodymium isotopes of the eastern US GEOTRACES Equatorial Pacific Zonal Transect (GP16). Earth Planet. Sci. Lett. 576, 117233.
- Hatje, V., Bruland, K.W., Flegal, A.R., 2014. Determination of rare earth elements after pre-concentration using NOBIAS-chelate PA-1®resin: method development and application in the San Francisco Bay plume. Mar. Chem. 160, 34–41.
- Hongo, Y., Obata, H., Sotto Alibo, D., Nozaki, Y., 2006. Spatial variations of rare earth elements in North Pacific surface water. J. Oceanogr. 62, 441–455.
- Jeandel, C., Delattre, H., Grenier, M., Pradoux, C., Lacan, F., 2013. Rare earth element concentrations and Nd isotopes in the Southeast Pacific Ocean. Geochem. Geophys. Geosystems 14, 328–341.
- Jia, Q., Li, T., Xiong, Z., Steinke, S., Algeo, T.J., Jiang, F., Chang, F., Qin, B., 2020. Thermocline dynamics in the northwestern tropical Pacific over the past 700 kyr. Quat. Sci. Rev. 244, 106465.
- Jickells, T.D., An, Z.S., Andersen, K.K., Baker, A.R., Bergametti, G., Brooks, N., Cao, J.J., Boyd, P.W., Duce, R.A., Hunter, K.A., Kawahata, H., Kubilay, N., laRoche, J., Liss, P. S., Mahowald, N., Prospero, J.M., Ridgwell, A.J., Tegen, I., Torres, R., 2005. Global iron connections between desert dust, ocean biogeochemistry, and climate. Science 308, 67–71.
- Kaneko, I., Takatsuki, Y., Kamiya, H., Kawae, S., 1998. Water property and current distributions along the WHP-P9 section (137°-142°) in the western North Pacific. J. Geophys. Res. Oceans 103, 12959–12984.
- Karstensen, J., Tomczak, M., 1998. Age determination of mixed water masses using CFC and oxygen data. J. Geophys. Res. 103, 18599–18609.
- Kawabe, M., Fujio, S., 2010. Pacific Ocean circulation based on observation. J. Oceanogr. 66, 389–403.
- Kawabe, M., Fujio, S., Yanagimoto, D., 2003. Deep-water circulation at low latitudes in the western North Pacific. Deep Sea Res. Part Oceanogr. Res. Pap. 50, 631–656.
- Kawabe, M., Fujio, S., Yanagimoto, D., Tanaka, K., 2009. Water masses and currents of deep circulation southwest of the Shatsky Rise in the western North Pacific. Deep Sea Res. Part Oceanogr. Res. Pap. 56, 1675–1687.
- Kishi, M.J., Okunishi, T., Yamanaka, Y., 2004. A comparison of simulated particle fluxes using NEMURO and other ecosystem models in the Western North Pacific. J. Oceanogr. 60, 63–73.
- Klinkhammer, G., Elderfield, H., Hudson, A., 1983. Rare-earth elements in seawater near hydrothermal vents. Nature 305, 185–188.
- Klinkhammer, G.P., Elderfield, H., Edmond, J.M., Mitra, A., 1994. Geochemical implications of rare earth element patterns in hydrothermal fluids from mid-ocean ridges. Geochim. Cosmochim. Acta 58, 5105–5113.
- Labasque, T., Chaumery, C., Aminot, A., Kergoat, G., 2004. Spectrophotometric Winkler determination of dissolved oxygen: re-examination of critical factors and reliability. Mar. Chem. 88 (1–2), 53–60.
- Labatut, M., Lacan, F., Pradoux, C., Chmeleff, J., Radic, A., Murray, J.W., Poitrasson, F., Johansen, A.M., Thil, F., 2014. Iron sources and dissolved-particulate interactions in the seawater of the Western Equatorial Pacific, iron isotope perspectives. Glob. Biogeochem. Cycles 28, 1044–1065.
- Lacan, F., Jeandel, C., 2001. Tracing Papua New Guinea imprint on the central Equatorial Pacific Ocean using neodymium isotopic compositions and rare earth element patterns. Earth Planet. Sci. Lett. 186, 497–512.
- Lambelet, M., van de Flierdt, T., Crocket, K., Rehkämper, M., Kreissig, K., Coles, B., Rijkenberg, M.J.A., Gerringa, L.J.A., de Baar, H.J.W., Steinfeldt, R., 2016. Neodymium isotopic composition and concentration in the western North Atlantic Ocean: results from the GEOTRACES GA02 section. Geochim. Cosmochim. Acta 177, 1–29.
- Letelier, R.M., Björkman, K.M., Church, M.J., Hamilton, D.S., Mahowald, N.M., Scanza, R.A., Schneider, N., White, A.E., Karl, D.M., 2019. Climate-driven oscillation of phosphorus and iron limitation in the North Pacific Subtropical Gyre. Proc. Natl. Acad. Sci. 116, 12720–12728.
- Li, X., Wu, K., Gu, S., Jiang, P., Li, H., Liu, Z., Dai, M., 2021a. Enhanced biodegradation of dissolved organic carbon in the western boundary Kuroshio current when intruded to the marginal South China Sea. J. Geophys. Res. Oceans 126.
- Li, S., Zhong, Y., Zhou, M., Wu, H., Zhang, Z., Li, B., Gao, Y., 2021b. Mixed layer water mass analysis on the East China Sea inner shelf. Estuar. Coast. Shelf Sci. 261, 107561.

- Li, H., Xie, G., Zhao, J., Hu, Z., Cui, X., Zhang, H., 2022. Optimum multiparameter analysis of water mass structure off western Guangdong during spring monsoon transition. Water 14, 375.
- Liu, Q., Zhang, J., He, H., Ma, L., Li, H., Zhu, S., Matsuno, T., 2022. Significance of nutrients in oxygen-depleted bottom waters via various origins on the mid-outer shelf of the East China Sea during summer. Sci. Total Environ. 826, 154083.
- Lupton, J.E., Pyle, D.G., Jenkins, W.J., Greene, R., Evans, L., 2004. Evidence for an extensive hydrothermal plume in the Tonga-Fiji region of the South Pacific. Geochem. Geophys. Geosyst. 5, Q01003.
- Lupton, J., Rubin, K.H., Arculus, R., Lilley, M., Butterfield, D., Resing, J., Baker, E., Embley, R., 2015. Helium isotope, C/ <sup>3</sup>He, and Ba-Nb-Ti signatures in the northern Lau Basin: Distinguishing arc, back-arc, and hotspot affinities: Helium and Carbon in Northern Lau Basin. Geochem. Geophys. Geosyst. 16, 1133–1155.
- Macdonald, A.M., Mecking, S., Robbins, P.E., Toole, J.M., Johnson, G.C., Talley, L., Cook, M., Wijffels, S.E., 2009. The WOCE-era 3-D Pacific Ocean circulation and heat budget. Prog. Oceanogr. 82, 281–325.
- McCartney, M.S., 1977. Subantarctic mode water. Deep-Sea Res. 24, 103-119.
- Michard, A., 1989. Rare earth element systematics in hydrothermal fluids. Geochim. Cosmochim. Acta 53, 745–750.
- Michard, A., Albarède, F., Michard, G., Minster, J.F., Charlou, J.L., 1983. Rare-earth elements and uranium in high-temperature solutions from East Pacific Rise hydrothermal vent field (13 °N). Nature 303, 795–797.
- Mitra, A., Elderfield, H., Greaves, M.J., 1994. Rare earth elements in submarine hydrothermal fluids and plumes from the Mid-Atlantic Ridge. Mar. Chem. 46, 217–235.
- Molina-Kescher, M., Frank, M., Hathorne, E., 2014. South Pacific dissolved Nd isotope compositions and rare earth element distributions: Water mass mixing versus biogeochemical cycling. Geochim. Cosmochim. Acta 127, 171–189.
- Molina-Kescher, M., Hathorne, E.C., Osborne, A.H., Behrens, M.K., Kölling, M., Pahnke, K., Frank, M., 2018. The influence of basaltic islands on the oceanic REE distribution: a case study from the tropical South Pacific. Front. Mar. Sci. 5, 50.
- Naveira Garabato, A.C., Heywood, K.J., Stevens, D.P., 2002. Modification and pathways of Southern Ocean Deep Waters in the Scotia Sea. Deep Sea Res. Part I Oceanogr. Res. Pap. 49, 681–705.
- Nishioka, J., Obata, H., 2017. Dissolved iron distribution in the western and central subarctic Pacific: HNLC water formation and biogeochemical processes. Limnol. Oceanogr. 62, 2004–2022.
- Nozaki, Y., Alibo, D.-S., Amakawa, H., Gamo, T., Hasumoto, H., 1999. Dissolved rare earth elements and hydrography in the Sulu Sea. Geochim. Cosmochim. Acta 63, 2171–2181.
- Osborne, A.H., Haley, B.A., Hathorne, E.C., Plancherel, Y., Frank, M., 2015. Rare earth element distribution in Caribbean seawater: continental inputs versus lateral transport of distinct REE compositions in subsurface water masses. Mar. Chem. 177, 172–183.
- Paffrath, R., Pahnke, K., Böning, P., Rutgers van der Loeff, M., Valk, O., Gdaniec, S., Planquette, H., 2021. Seawaterr-particle interactions of rare earth elements and neodymium isotopes in the deep Central Arctic Ocean. J. Geophys. Res. Oceans 126, e2021JC017423.
- Pearce, C.R., Jones, M.T., Oelkers, E.H., Pradoux, C., Jeandel, C., 2013. The effect of particulate dissolution on the neodymium (Nd) isotope and Rare Earth Element (REE) composition of seawater. Earth Planet. Sci. Lett. 138–147.
- Qu, T., Lindstrom, E.J., 2004. Northward intrusion of Antarctic Intermediate Water in the Western Pacific. J. Phys. Oceanogr. 34, 2104–2118.
- Qu, T., Mitsudera, H., Yamagata, T., 1998. On the western boundary currents in the Philippine Sea. J. Geophys. Res. Oceans 103, 7537–7548.
- Qu, T., Girton, J.B., Whitehead, J.A., 2006. Deepwater overflow through Luzon Strait. J. Geophys. Res. Oceans 111, C01002.
- Reid, J.L., 1997. On the total geostrophic circulation of the Pacific Ocean: flow patterns, tracers, and transports. Prog. Oceanogr. 39, 263–352.
- Ren, Z.Y., Hanyu, T., Miyazaki, T., Chang, Q., Kawabata, H., Takahashi, T., Hirahara, Y., Nichols, A.R.L., Tatsumi, Y., 2009. Geochemical differences of the Hawaiian Shield Lavas: Implications for melting process in the heterogeneous Hawaiian plume. J. Petrol. 50. 1553–1573.
- Rudnicki, M.D., Elderfield, H., 1993. A chemical model of the buoyant and neutrally buoyant plume above the TAG vent field, 26 degrees N, mid-Atlantic ridge. Geochim. Cosmochim. Acta 57, 2939–2957.
- Sabine, C.L., Feely, R.A., Gruber, N., Key, R.M., Lee, K., Bullister, J.L., Wanninkhof, R., Wong, C.S., Wallace, W.R., Tilbrook, B., Millero, F.J., Peng, T.-H., Kozyr, A., Onon, T., Rios, A.F., 2004. The oceanic sink for anthropogenic CO<sub>2</sub>. Science 305, 367–371.
- Schijf, J., Christenson, E.A., Byrne, R.H., 2015. YREE scavenging in seawater: a new look at an old model. Mar. Chem. 177, 460–471.
- Schlitzer, R., 2016. Ocean Data View. http://odv.awi.de.
- Sherrell, R.M., Field, M.P., Ravizza, G., 1999. Uptake and fractionation of rare earth elements on hydrothermal plume particles at 9 degrees 45' N, East Pacific Rise. Geochim. Cosmochim. Acta 63, 1709–1722.
- Shiller, A.M., Chan, E.W., Joung, D.J., Redmond, M.C., Kessler, J.D., 2017. Light rare earth element depletion during Deepwater Horizon blowout methanotrophy. Sci. Rep. 7, 10389.
- Sholkovitz, E.R., Elderfield, H., Szymczak, R., Casey, K., 1999. Island weathering: river sources of rare earth elements to the Western Pacific Ocean. Mar. Chem. 68, 39–57.
- Singh, S.P., Singh, S.K., Goswami, V., Bhushan, R., Rai, V.K., 2012. Spatial distribution of dissolved neodymium and €Nd in the Bay of Bengal: Role of particulate matter and mixing of water masses. Geochim. Cosmochim. Acta 94, 38–56.

- Stichel, T., Hartman, A.E., Duggan, B., Goldstein, S.L., Scher, H., Pahnke, K., 2015.
  Separating biogeochemical cycling of neodymium from water mass mixing in the Eastern North Atlantic. Earth Planet. Sci. Lett. 412, 245–260.
- Stichel, T., Pahnke, K., Duggan, B., Goldstein, S.L., Hartman, A.E., Paffrath, R., Scher, H. D., 2018. TAG Plume: Revisiting the hydrothermal neodymium contribution to seawater. Front. Mar. Sci. 5, 96.
- Suga, T., Kato, A., Hanawa, K., 2000. North Pacific Tropical Water: its climatology and temporal changes associated with the climate regime shift in the 1970s. Prog. Oceanogr. 47, 223–256.
- Sverjensky, D.A., 1984. Europium redox equilibria in aqueous solution. Earth Planet. Sci. Lett. 67, 70–78.
- Tagliabue, A., Bopp, L., Dutay, J.-C., Bowie, A.R., Chever, F., Jean-Baptiste, P., Bucciarelli, E., Lannuzel, D., Remenyi, T., Sarthou, G., Aumont, O., Gehlen, M., Jeandel, C., 2010. Hydrothermal contribution to the oceanic dissolved iron inventory. Nat. Geosci. 3, 252–256.
- Takahashi, Y., Châtellier, X., Hattori, K.H., Kato, K., Fortin, D., 2005. Adsorption of rare earth elements onto bacterial cell walls and its implication for REE sorption onto natural microbial mats. Chem. Geol. 219, 53–67.
- Takata, H., Tagami, K., Aono, T., Uchida, S., 2009. Determination of trace levels of yttrium and rare earth elements in estuarine and coastal waters by Inductively Coupled Plasma Mass Spectrometry following preconcentration with NOBIAS-CHELATE resin. At. Spectrosc. 30, 11–19.
- Talley, L.D., 1993. Distribution and formation of North Pacific Intermediate Water. J. Phys. Oceanogr. 23, 517–537.
- Talley, L.D., Nagata, Y., Fujimura, M., Iwao, T., Kono, T., Inagake, D., Hirai, M., Okuda, K., 1995. North Pacific intermediate water in the Kuroshio/Oyashio mixed water region. J. Phys. Oceanogr. 25, 475–501.
- Talley, L.D., Pickard, G.L., Emery, W.J., 2011. Descriptive physical oceanography: an introduction, sixth ed. Academic Press, Amsterdam, Boston.
- Taylor, S.R., McLennan, S.M., 1985. The continental crust, its composition and evolution:
  An examination of the geochemical record preserved in sedimentary rocks.
  Blackwell Scientific, Oxford.
- Tian, Z., Zhou, C., Xiao, X., Wang, T., Qu, T., Yang, Q., Zhao, W., Tian, J., 2021. Water-mass properties and circulation in the deep and abyssal Philippine Sea. J. Geophys. Res. Oceans 126, e2020JC016994.
- Tomczak, M., Large, D.G.B., 1989. Optimum multiparameter analysis of mixing in the thermocline of the eastern Indian Ocean. J. Geophys. Res. 94, 16141.
- Toole, J.M., Millard, R.C., Wang, Z., Pu, S., 1990. Observations of the Pacific North Equatorial Current bifurcation at the Philippine coast. J. Phys. Oceanogr. 20, 307–318.
- Tsunogai, S., Ono, T., Watanabe, S., 1993. Increase in total carbonate in the western North Pacific water and a hypothesis on the missing sink of anthropogenic carbon. J. Oceanogr. 49, 305–315.
- Von Damm, K.L., 1990. Seafloor hydrothermal activity: black smoker chemistry and chimneys. Annu. Rev. Earth Planet. Sci 18. 173–204.
- Wang, F., Zang, N., Li, Y., Hu, D., 2015. On the subsurface countercurrents in the Philippine Sea. J. Geophys. Res. Oceans. 120, 131–144.
- Wang, F., Song, L., Li, Y., Liu, C., Wang, J., Lin, P., Yang, G., Zhao, J., Diao, X., Zhang, D., Hu, D., 2016. Semiannually alternating exchange of intermediate waters east of the Philippines. Geophys. Res. Lett. 43, 7059–7065.
- Welschmeyer, N.A., 1994. Fluorometric analysis of chlorophyll a in the presence of chlorophyll b and pheopigments. Limnol. Oceanogr. 39, 1985–1992.
- Wu, J., Wells, M.L., Rember, R., 2011. Dissolved iron anomaly in the deep tropical-subtropical Pacific: Evidence for long-range transport of hydrothermal iron. Geochimica et Cosmochimica Acta 75, 460–468.
- Xu, B., Li, S., Burnett, W.C., Zhao, S., Santos, I.R., Lian, E., Chen, X., Yu, Z., 2022. Radium-226 in the global ocean as a tracer of thermohaline circulation: Synthesizing half a century of observations. Earth Sci. Rev. 226, 103956.
- Xu, F.H., Oey, L.Y., 2014. State analysis using the Local Ensemble Transform Kalman Filter (LETKF) and the three-layer circulation structure of the Luzon Strait and the South China Sea. Ocean Dyn. 64, 905–923.
- You, Y., 2003. The pathway and circulation of North Pacific Intermediate Water: the pathway and circulation of NPIW. Geophys. Res. Lett. 30, 2291.
- Yücel, M., Gartman, A., Chan, C.S., Luther, G.W., 2011. Hydrothermal vents as a kinetically stable source of iron-sulphide-bearing nanoparticles to the ocean. Nat. Geosci. 4, 367–371.
- Zang, N., Wang, F., Sprintall, J., 2020. The intermediate water in the Philippine Sea. J. Ocean. Limnol. 38, 1343–1353.
- Zenk, W., Siedler, G., Ishida, A., Holfort, J., Kashino, Y., Kuroda, Y., Miyama, T., Müller, T.J., 2005. Pathways and variability of the Antarctic Intermediate Water in the western equatorial Pacific Ocean. Prog. Oceanogr. 67, 245–281.
- Zhai, F., Gu, Y., 2020. Abyssal circulation in the Philippine Sea. J. Ocean Univ. China 19, 249–262.
- Zhang, J., Amakawa, H., Nozaki, Y., 1994. The comparative behaviors of yttrium and lanthanides in the seawater of the North Pacific. Geophys. Res. Lett. 21, 2677–2680.
- Zhang, L., Hui, Y., Qu, T., Hu, D., 2021. Seasonal variability of subthermocline eddy kinetic energy East of the Philippines. J. Phys. Oceanogr. 51, 685–699.
- Zhang, Y., Lacan, F., Jeandel, C., 2008. Dissolved rare earth elements tracing lithogenic inputs over the Kerguelen Plateau (Southern Ocean). Deep Sea Res. Part II Top. Stud. Oceanogr. 55, 638–652.
- Zhang, J., Nozaki, Y., 1996. Rare earth elements and yttrium in seawater: ICP-MS determinations in the East Caroline, Coral Sea, and South Fiji basins of the western South Pacific Ocean. Geochim. Cosmochim. Acta 60, 4631–4644.
- Zhang, J., Liu, Q., Bai, L., Matsuno, T., 2018. Water mass analysis and contribution estimation using heavy rare earth elements: significance of Kuroshio intermediate water to Central East China Sea shelf water. Mar. Chem. 204, 172–180.

- Zhang, Q., Zhou, H., Liu, H., 2012. Interannual variability in the Mindanao Eddy and its impact on thermohaline structure pattern. Acta Oceanol. Sin. 31, 56-65.
- Zhang, R., Zhu, X., Yang, C., Ye, L., Zhang, G., Ren, J., Wu, Y., Liu, S., Zhang, J., Zhou, M., 2019. Distribution of dissolved iron in the Pearl River (Zhujiang) Estuary and the northern continental slope of the South China Sea. Deep Sea Res. Part II Top. Stud. Oceanogr. 167, 14–24.
  Zheng, L., Sohrin, Y., 2019. Major lithogenic contributions to the distribution and budget
- of iron in the North Pacific Ocean. Sci. Rep. 9, 11652.
- Zheng, X.Y., Plancherel, Y., Saito, M.A., Scott, P.M., Henderson, G.M., 2016. Rare earth elements (REEs) in the tropical South Atlantic and quantitative deconvolution of their non-conservative behavior. Geochim. Cosmochim. Acta 177, 217–237.
- Zindler, A., Hart, S.R., Frey, F.A., Jakobsson, S.P., 1979. Nd and Sr isotope ratios and rare earth element abundances in Reykjanes Peninsula basalts evidence for mantle heterogeneity beneath Iceland. Earth Planet. Sci. Lett. 45, 249–262.